J Fail. Anal. and Preven.
https://doi.org/10.1007/s11668-023-01628-5

TECHNICAL ARTICLE—PEER-REVIEWED

Numerical Investigation of the Failure of Stiffened Steel Plates Subjected to Near-Field Blast Loads

Nurul Syafiqah Abdul Razak · Aizat Alias · Nor Maslina Mohsan · Siti Aliyyah Masjuki

Submitted: 14 September 2022 / in revised form: 25 February 2023 / Accepted: 3 March 2023

Abstract This paper study the failure of stiffened steel plates subjected to near-filed blast loads using finite element (FE) analysis. Half-symmetry 3D FE models were developed using Abaqus for unstiffened and stiffened steel plates with different stiffeners configurations and sizes were used using solid brick elements. The behaviour of steel plates was modelled using classical plasticity constitutive equation, and the failure of the plates was modelled using ductile damage criterion. The influence of strain rates was considered using the Cowper–Symonds equation. The blast loads were applied using CONWEP function in Abaqus. The FE model of unstiffened plates was verified and validated against experimental data from literature where a good agreement was achieved. The FE model then was extended to incorporate different sizes and configurations of stiffeners. The study observed that stiffened steel plate tends to fail at lower blast pressure. The failure is influenced by the position and arrangement of stiffeners with respect to the size of stiffeners. Two new sub-modes of failure for stiffened steel plates are proposed namely Mode II*s and Mode IIs for partial plate tearing along stiffener and rupture of stiffener, respectively.

Keywords Stiffened steel plate · Ductile damage · Finite element · Damage energy

Introduction

Stiffened steel plates are used in many applications such as blast walls for offshore structures, military vehicles and ship hull as stiffened plates have higher stiffness compared unstiffened or bare steel plates. In general applications, these plates may subject to known design static load but in extreme condition such as blast due to explosions, the actual loads impacted on the plates may be unknown because of various factors. The response of steel plates subjected to blast loads have been the subject of interest for many years and still on going.

Yuen et al. [1] has provided an extensive review on this subject where the authors compiled and discussed the progress of this subject for more than 20 years of research. The discussion focussed on the dynamic behaviour, modes of failure and dimensional analysis of unstiffened and stiffened steel plates subjected uniform and localised blast loads for various shape of steel plates from experimental programs. The modes of failure in stiffened plates are influenced by types of loading [2, 3, 4] and boundary conditions [5]. Henchie et al. [6] studied the response of circular plates subjected to repeated uniform blasts and the results show the mid-point displacement increases per applied loads. Yuen et al. [7] investigated the response of

This article is an invited paper selected from presentations at the 6th Symposium on Damage Mechanism in Materials and Structures (SDMMS 2022), held August 16–17, 2022 in Kuantan, Malaysia. The manuscript has been expanded from the original presentation. The special issue was organized by Nasrul Azuan Alang, Norhaida Ab Razak, and Aizat Alias, Universiti Malaysia Pahang.

N. S. A. Razak · A. Alias (✉)
Faculty of Civil Engineering Technology, Universiti Malaysia Pahang, Gambang, Kuantan, Pahang, Malaysia
e-mail: aizat@ump.edu.my

N. M. Mohsan
Faculty of Civil Engineering, Universiti Teknologi MARA Pahang, Jengka, Pahang, Malaysia

S. A. Masjuki
Department of Civil Engineering, Kuliyyah of Engineering, International Islamic University, Kuala Lumpur, Malaysia

Published online: 23 March 2023

V-shaped steel plates at near-field explosion in which the results revealed smaller included angle deflected more gas pressure and as a result, reduces the mid-point deflection of the plate. However, this small, included angle may resulted in instability as it increases the plate centre of gravity. Recently, Rigby et al. [8] study the influence of spherical and cylindrical charge shapes on the deflection of near-field blast-loaded plates and the results revealed that there is a different deformation profiles from two different charge shapes. The study then proposes a methodology for spherical equivalence of cylindrical explosive with the main aim is to provide a simplified tool to model the effects of charge shape.

The modes of failure for steel plates subjected to blast loads have been compiled by Jacob et al. [2] from multiple sources of previous studies. In general, there are four 4 modes of failure, and they are large plastic deformation (Mode I), tearing of the plate at central area and boundary (Mode II), transverse shear failure (Mode III) and petalling, which the plate folded outward. Mode I and Mode II have more sub-modes of failure depending on the types of loading where all these modes of failure are tabulated in Table 1 according to Jacob et al. [2]. The modes of failure in Table 1 focusses on the failure of unstiffened steel plates. The study by Langdon et al. [4] has observed additional failures, a part from Mode 1 and petalling, which are thinning of plate at central area, partial tearing of the plate along the stiffener and rupture of stiffeners. These additional modes of failure have not been introduced in the modes of failure as in Table 1.

Previous studies have shown that the presence of stiffeners improves the performance of steel plates when subjected to blast loads [6, 7]. Gan et al. [6] found that the residual displacement and support rotation angle decrease linearly when the number and size of stiffeners increases. Razak and Alias [9] also observed that the maximum displacement of stiffened plates reduced as the configuration of the stiffeners were changed from a single stiffener to cross stiffeners. The performance of stiffened steel plates could be improved by increasing the numbers and sizes of the stiffeners [10] as such it could improve the energy absorption of the stiffened plates [11]. The study by Langdon et al. [4], however, has shown that the presence of stiffeners has caused the steel plates to fail at a lower blast load when compared to unstiffened steel plates under localised blast loading [4]. The authors have confirmed this behaviour thorough their numerical simulations using finite element analysis. They have performed the numerical analysis by incorporating temperature-dependent material properties to predict the tearing of the plate through high-temperature bands. Moreover, they also observed the failure based on the stretching of the elements. Langdon et al. [4] suggests the local increase in stiffness at the plate-stiffener edges was the caused the plates failure at lower blast impulse. The study, however, was limited to two sizes of stiffeners only which were 3 × 5 mm and 3 × 7 mm.

Bonorchis and Nurick [12] studied the response of steel plates stiffened with welded connection subjected to near-field blast loads where the effect of stress relieving, stiffeners height and welding configurations were the studied. The study revealed that increasing the stiffeners height

Table 1 Modes of failure for plates subjected to different blast loads [2]

Modes of failure	Sub-modes of failure	Description of the failure	Types of blast load	
			Uniform	Localised
I	Mode I	Large plastic deformation	Y	Y
	Mode Ia	Large plastic deformation with necking around part of the boundary	Y	
	Mode Ib	Large plastic deformation with necking around the entire boundary	Y	Y
	Mode Itc	Large plastic deformation with thinning in the central area		Y
II	Mode II	Tensile tearing at the boundary	Y	Y
	Mode II*	Large plastic deformation with partial tearing around part of the boundary	Y	
	Mode II*c	Partial tearing in the central area		Y
	Mode IIa	Tearing with increasing mid-point deflection with increasing impulse with complete tearing at the boundary	Y	
	Mode IIb	Tearing with decreasing mid-point deflection with increasing impulse with complete tearing at the boundary	Y	
	Mode IIc	Complete tearing in the central area capping		Y
III	Mode III	Transverse shear failure at the boundary	Y	
IV	Petalling	Tearing at the centre with 'petals' of material folded away from blast location		Y

reduced the tearing threshold of the steel plate. The failure of stiffened steel plates at lower blast impulse was not only observed in open air blast but also occurred on stiffened steel plates subjected to internal blast loads as studied by Li et al. [13]. The study suggests the presence of stiffeners lowered the damage threshold of the stiffened steel plates and the failure mostly occur at the plate-stiffener intersections. Additionally, they suggest stiffeners have great effect to steel plates when the dominant behaviour is bending but less significant effect when membrane action is dominant. Meanwhile, Gan et al. [10] proposes that the characteristic of the stiffeners might change the modes of damage of stiffened steel plates in which the stiffeners confined the failure in between the stiffeners spacing whereas unstiffened steel plate would endure breach failure or completely destroyed under certain blast pressure. These previous studies, however, have not discussed in detail the reason that could cause stiffened steel plates to have lower damage threshold and as a result, fail at a lower blast impulse compared to unstiffened steel plates.

Experimental program, analytical and numerical methods have been used by researcher to gain insight to the behaviour, response and failure of structures subjected to blast loads. Experimental works could be considered as the well-founded method to investigate and assess the response and failure of structures subjected to blast loads. The method, however, suffers several issues such as reproducibility of similar results [14], missing data due to the failure of measuring devices [15], costly and time consuming [16]. Analytical method such as rigid-plastic analysis provides a very quick estimation but limited to the prediction of permanent transverse displacement only [17]. Numerical modelling provides an alternative to gain insights into the behaviour of structures subjected to blast loads in a more detail manner and this advantage has been utilised by researcher such as Gan et al. [10] to obtain the maximum displacement of their specimens as their measuring tools in the field test were damaged due to the blast wave. Coupled Eulerian–Lagrangian (CEL), Uncoupled Eulerian–Lagrangian (UEL) and Langrangian formulations are three techniques that are commonly used by researchers for numerical modelling [7, 18, 19]. Each of these methods has their advantages and disadvantages where for example the CEL method use fluid–structure interaction formulation to model the interaction between the blast wave and structure while for UEL method, the blast incident is modelled in Eulerian domain using computational fluid dynamic (CFD) and then translated or remapped the blast wave pressure onto the target structure, which is modelled using Lagrangian formulation. The former is the most complex and could be considered as the most realistic, while the latter is slightly less complex method and close to the real situation. These two methods, however, require expensive computer resources where the larger or detail the model, the longer it will take to complete the computational process [20].

The Lagrangian formulation or technique is the simplest modelling technique to simulate and investigate the response of structures subjected to blast loads. In pure Lagrangian formulation, the propagation of blast wave is neglected because the Eulerian formulation is not in used. Using Lagrangian formulation, the blast loads would be simplified in several different methods. One of the methods is by applying pressure directly on the structures either using built-in pressure function [3] or using user-subroutine [21] where the blast pressure time history, which could be described as instantaneous rise of pressure then followed by exponential decay of pressure, is simplified in the shape of rectangular or triangular shape by maintaining the blast impulse [22, 23]. Micallef et al. [17, 21] and Mehreganian et al. [22] used as a specific blast load spatial distribution with rectangular temporal blast function to investigate the response of circulate steel plates subjected to localised blast loading. The results from their numerical analysis were in a good agreement with their proposed analytical rigid-plastic formulations. Another simplified blast load function in Langrangian formulation is by using CONWEP blast load built-in function, which is available in commercial finite element software such as ANSYS and Abaqus. The CONWEP was developed according to the Kingery and Bulmash empirical equation by Randers-Pherson and Bannister [24] in which the reflected blast pressure–time history is based on the Friedlander equation [25]. With CONWEP, the modelling of the propagation of blast wave in surrounding medium and interaction of the blast wave and structure in the model are not necessitate and this help to accelerate the simulation. Consequently, the influence of blast wave such as clearing, diffraction or rarefaction [26] as well as afterburning effect and structure-fireball interaction under localised blast conditions [27, 28] are not available in the blast load function due to the simplicity of the CONWEP blast load function. Lomazzi et al. [27] suggests the influences of afterburning effect and structure-fireball interactions have to be included in more advanced and complex numerical model as their CEL and Lagrangian formulations using CONWEP were unable to predict quite well the response of steel plates when the scaled distance $Z < 0.6$ m/kg$^{1/3}$.

In contrast, some of the studies that used CONWEP to simulate blast loads on structures with scaled distance. $Z < 0.6$ m/kg$^{1/3}$ have shown a comparable result when compared to experimental data. Lin and co-researcher [29] successfully modelled a blast test on a reinforced concrete (RC) panel with a scaled distance of 0.46 m/kg$^{1/3}$ using CONWEP as the blast load simulator. The deflection of the RC panel from the finite element analysis was closed to the

measured field data. Dharmasena et al. [30] performed numerical analysis of sandwich plates subjected to 1–3 kg of TNT at 0.1 mm distance ergo, the scaled distances of the study were between 0.06 and 0.1 m/kg$^{1/3}$. They used CONWEP to model the blast loads and the results were comparable with the experimental results. Spranghers et al. [31] studied the dynamic response of aluminium plates subjected to 0.04 kg of C4 at 0.25 m standoff distance (Z = 0.07 m/kg$^{1/3}$, with the TNT equivalent factor of 1.34) under air-free explosions. The study compared the reflected pressure from CONWEP and final plate deformation where they found that the numerical results agree quite well with the experiment. In some cases, the CONWEP could produce a better result compared to more advance numerical technique. For instance, Nelson et al. [32] compared the circumferential strain of a cylindrical composite structure using CONWEP, CONWEP-ALE coupling and full ALE technique in which the CONWEP gives the most accurate predicted circumferential strain with 12% difference against test data. The test was conducted using 0.135 kg of TNT placed at 0.161 m distance from the plate (Z = 0.31 m/kg$^{1/3}$). Rigby et al. [33] conducted a control experimental program to develop a methodology to measure blast pressure at near-field blast loads. The scaled distances to the centre of the plate were 0.15 and 0.25 m/kg$^{1/3}$ to the radial pressure bar mounted flush with the face of the plate. The study recorded oscillation of the pressure–time histories due to Pochammer–Chree dispersion and for comparison with their Arbitrary Lagrangian–Eulerian (ALE) and CONWEP results, the dispersion was corrected to obtain a more precise character of peak overpressure. Surprisingly, the pressure–time histories predicted by CONWEP in Rigby's agree fairly with the corrected near-field blast pressure which is in contrast to the common conjecture that CONWEP is less accurate for near-field blasts. According to these studies, it might be reasonable to postulate that CONWEP is a decent and sound tool to investigate structures subjected to near-field blast loads.

This study focuses on the use of CONWEP to model localised blast loads on unstiffened and stiffened steel plates to gain insights into the damage threshold and failure mechanism of stiffened steel plates especially when the plates fail at lower blast impulse as compared to unstiffened steel plates under localised blast loading. The size of stiffeners and configurations were the main parameters investigated in this study. CONWEP was used to model the localised blast loads as it could provide fast and reliable results [31]. The discussion in the subsequent section includes the predicted damage energy from the numerical analysis to have a better understanding on the damage and failures of stiffened steel plates as this study incorporated material failure criterion with element deletion technique to model the failure of the stiffened steel plates. Lastly, based on the numerical observation, new sub-modes of failure could be introduced to consider the failure of the plates and stiffeners.

Methodology

This numerical study used Abaqus, a finite element (FE) software, to study the dynamic behaviour and model the failure of steel plates subjected to near-field blast loads. Initially, this study developed a half-symmetry 3D finite element model according to an experimental study of unstiffened steel plates subjected to near-field blast loads conducted by Yuen et al. [34]. The unstiffened FE model was verified and validated against the test data. The validated FE model then was extended by incorporating stiffeners with various configuration and sizes.

Description of the Experiment

Yuen et al. [34] conducted an experimental study on the influence of orientation of blast loading on a square steel plate in two different settings. The first setting was where the plate was titled at two different angles with respect to the explosive. For the second setting, the explosive disc with 38 mm of diameter was tilted in four different angles with respect to the plate. The square steel plate was made from Domex steel with 2 mm thickness and mounted using 20-mm-thick clamps on a horizontal ballistic pendulum test rig (Refer to Yuen et al. [34] for detail). Due to the clamp's width, the exposed area of the plate was 300 mm by 300 mm. The reported yield strength of the Domex steel was 222 MPa obtained after uniaxial tensile tests. The standoff distance between the explosive and the plate was fixed at 40 mm, and the explosive was made from Plastic Explosive No. 4 (PE4). The charge mass was varied between 8 and 28 g.

Finite Element Model

3D finite element models of stiffened and unstiffened steel plates were developed in Abaqus/CAE. Half-symmetry models were used in this study, taking the advantage of symmetrical condition of the steel plates and clamps. The plate, the clamps and the bolts were modelled using solid, linear eight-node brick elements with reduced integration and hourglass control (C3D8R). The interactions between the plate, the clamps and the bolts were defined using contact pair algorithm in Abaqus. The normal and tangential behaviour of the surface-to-surface interactions between these components was defined using 'hard' contact formulation and penalty frictional formulation, respectively. The coefficient of friction for the tangential

behaviour was set as 0.3 for steel-steel interactions [7, 9]. A symmetry boundary condition was applied along the surface of the symmetrical boundary. In this numerical model, the clamps were assumed undeformed under the load; thus, the clamps were constrained for rotational and translational degree of freedoms. For the stiffened finite element (FE) steel plate prototype, the stiffeners were created from the same section of the steel plates by extruding the stiffener parts from the plate section with the assumption the stiffened plate prototypes would be manufactured using machining process similar to the process used by Yuen and Nurick [3] and Langdon et al. [4]. As a result, it was assumed the plate and the stiffeners prototype were unison and have the same material properties. The size of elements in FE models of stiffened steel plates was according to Mesh 5 setup. The finite element model setup is as depicted in Fig. 1.

Constitutive Equation

The constitutive material for the steel plate, stiffeners and the bolts were modelled using the classical plasticity model. The elastic limit was set at the yield strength and once exceeded the plate behaves plasticly with hardening. The yield strength of the plate was 222 MPa as reported in [34], and the stiffeners were assumed to have the same yield strength. The steel plates behaviour in tension and compression was assumed as bilinear relationship of elastic–plastic with hardening. On the other hand, it was assumed the clamps will not exceed their yield strength thus, the clamps were modelled as an elastic material, neglected their yield strength. The density of steel plates, stiffeners, bolts, and clamps was taken as 7850 kg/m^3 with the modulus of elasticity and the Poisson's ratio were assumed as 200 GPa and 0.3, respectively.

Steel is a material that sensitive to strain rate or also known as viscoplasticity material. The strain rate effect is known to increase the yield and ultimate tensile strength of steel. Hence, the modelling of this material property is very important in investigating the behaviour of steel structures subjected to blast loads. The influence of strain rate in numerical models is commonly simulated using the Cowper–Symonds model [35] or the Johnson–Cook model [18]. In this study, the Cowper–Symonds constitutive model was employed where the dynamic plastic strength is a function of static yield stress and strain rate as in Eq 1.

$$\sigma_y^{'} = \sigma_y \left\{ 1 + \left(\frac{\dot{\varepsilon}}{D} \right)^{1/q} \right\} \qquad \text{(Eq 1)}$$

where $\sigma_y^{'}$ is the dynamic flow stress, σ_y is the static yield stress and $\dot{\varepsilon}$ is the strain rate. The strain hardening coefficients, D and q, of the dynamic flow stress have to be known usually from uniaxial static test [18] or split Hopkinsion pressure bar (SHBT) [36, 37]. Different values of coefficients were reported as the Cowper–Symonds model is based on phenomenological approach [37–40]. However, the influence of these different coefficients' values could be considered as small according to Razak and Alias [35]. The most employed values for D and q are 40.4 and 5, respectively, which were employed in this study.

Steel is known to be a ductile material; hence, the damage of the steel plates was modelled using ductile damage model with element deletion algorithm to visualize the failure of the steel plates. These two settings are available in Abaqus library. The initiation criterion of

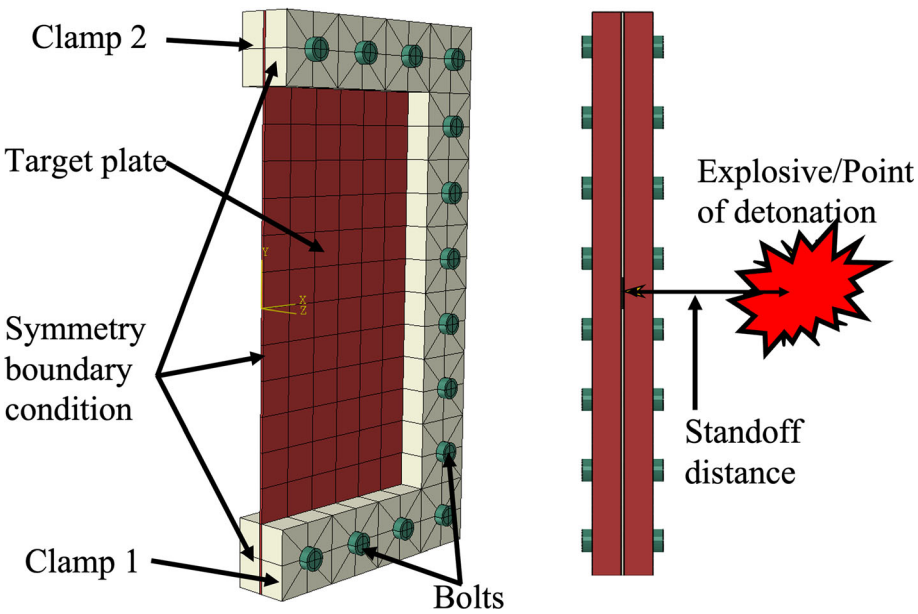

Fig. 1 3D half-symmetry finite element model setup

damage for ductile metal such as steels is predicted according to phenomenological model where the damage starts because of the nucleation, growth and coalescence of voids. The ductile damage model assumes that at the start of damage, the equivalent plastic strain is a function of strain rate and stress triaxiality. The damage evolves as the material hardness gradually degenerates and leads to material failure. The degradation of the materials is represented with scalar total damage variable. The scalar damage variable can be from 0, not damage, until 1.0, which represented full degradation of the hardness of the material. The damage elements are deleted when the maximum degradation, which is 1.0, is reached [41].

In this study, the onset of damage for steel plate and stiffeners was assumed when the equivalent plastic strain is equal to 0.25. The reason for this assumption is Yuen et al. [34] reported only the yield strength of their 2-mm Domex steel and no uniaxial tensile test results; hence, the actual fracture strain is not available. Curry and Langdon [16], however, have reported a set of uniaxial tensile test results of 3-mm Domex 355MC steel with an average yield strength of 450 MPa, which is higher that Yuen's. Nevertheless, the results from Curry and Langdon indicate the fracture strains of Domex 355MC are in the range of 0.2 and 0.25. As the Yuen's Domex is slightly lower in strength, it might be reasonable to postulate that the fracture strain of Yuen's Domex could be slightly higher because the ductility of steel with low yield strength is usually better than steel with higher steel strength due to lower amount of carbon content. The assumed fracture strain is similar to the fracture reported by Li et al. [42] for their steel, which has a yield strength of 345 MPa, just over Yuen's yield strength. It is known that, and it is evidence as reported by Curry and Langdon, the fracture strain for a similar type of steel could produce different fracture strain. Therefore, considering these factors it could be plausible to assume the onset of fracture strain for Yuen's Domex starts at 0.25 equivalent plastic strain.

Stress triaxiality is the ratio between hydrostatic pressure and Mises equivalent stress in which this stress has a marked influence to the formation of crack in different materials with different level of dependency [43]. Iqbal et al. [44] characterize mild steel round bars under different triaxial stress state, strain rate and temperature. The test shows that as the stress triaxiality increases, the fracture strain of the mild steel decreases exponentially. In other words, the ductility of mild steel decreases as the stress triaxiality increases. The increase in strain rate, although increases the mild steel strength, has caused the ductility of the mild steel to reduce. On the other hand, the test also revealed the increase in temperature reduces the mild steel strength, but there is an increase to the ductility as the specimen able to endure large amount of plastic deformation before cracks formed. For high strength low alloy steels, the rate of voids growth is influenced by the stress triaxiality where the voids grow rapidly as the stress triaxiality decreases and it is more pronounces at intermediate stress triaxiality [45]. Recently, Liu et al. [46] conducted an extensive study based on previous experimental data to investigate the influence of wide range stress triaxiality on different types of materials and validated the aptness of exponential function to simulate the void growth in fracture initiation model of ductile metals for low to medium stress triaxialities. These, studies have shown the importance of stress triaxialities in crack formation and its dependence to fracture strain. In this current study, however, the stress triaxiality is assumed to be constant throughout the entire prototype of the steel plate in this study. As there is no experimental data, the ratio used was 1.0 obtained from the exponential curve of fracture strain and stress triaxiality in Iqbal et al. [44] as the mild steel used in their test has a close yield strength to the Yuen's Domex steel.

Blast Load Modelling

The blast pressure–time history of an explosion is commonly represented using Friedlander equation. The blast pressure can be divided as incident peak overpressure and maximum reflected pressure. The former could be referred to the pressure of the explosion measured at a standoff distance (without any target). The latter is the pressure of the blast wave on objects or targets that are perpendicular to the direction of propagation and reflection of the blast wave. The incident pressure and the reflected overpressure could be modelled numerically using the Coupled Eulerian–Lagrangian domain [10] or Eulerian domain only [34] as both methods are influenced by the mesh quality and it requires quite a fine mesh depending on the size of the domain [47]. Therefore, both methods require quite a large computational resource.

In experiments, most of the times the reflected peak overpressure is the one that was measured or reported [48]. Abaqus library allows the reflected overpressure-time history to be obtained using Langrangian domain only using the CONWEP blast load function. The blast load function is in accordance with the function developed by Randers-Pherson and Bannister [24] which is given in Eq 2.

$$P(t) = P_r \cos^2\theta + P_m\left(1 + \cos^2\theta - 2\cos\theta\right) \qquad \text{(Eq 2)}$$

where P_r and P_m are the reflected and incident peak overpressure, respectively, and θ is the incident angle. A predefined target surface and a reference point, which act as the point of detonation, to determine the standoff distance and the angle of incident. This setting includes the definition of a type of explosion, either air or surface blast,

and the charge weight which the CONWEP requires to calculate the incident pressure and reflected peak overpressure. This blast load function, however, neglected the influence of shape and size of the explosive charge. The estimation of incident and reflected peak overpressure in CONWEP is according to the pressure produced by a detonation of trinitrotoluene (TNT) explosive material. As a result, any study that used other explosive materials requires to convert the mass of the explosive into TNT equivalent and input the value into the CONWEP blast load function. The experiment conducted by Yuen et al. [34] used PE4 discs as the explosive material. Several TNT equivalent conversion factors have been used or discussed in different studies such as 1.3 used by Yuen et al. [7], Sprangheres et al. [31] used 1.34 in their study and Xiao et al. [49] reported 1.2 and 1.37 from compilation of previous studies. Bogosian et al. [50] study suggests higher TNT equivalence is needed as the standoff distance become closer. They have proposed an empirical equation based on best-fit curves obtained from test data to estimate the TNT equivalent factor where the equation provide lower, median and upper bound factor based on the charge weight and standoff distance. Therefore, Bogosian's empirical function [50] was used to determine the TNT equivalent factor and the upper bound TNT equivalent factors were selected for this study. The reason for that is because, as suggested earlier, closer standoff distance requires higher TNT equivalent factor. In this study, the TNT equivalent factor of 1.82 was used and this has resulted the scaled distances, Z, to be in the range of 0.11–0.16 m/kg$^{1/3}$. This range of scaled distances is within the range as reported in Dharmasena et al. [30] and Spranghers et al. [31] which justified the used of CONWEP in this current study.

Results and Discussion

This section discusses the results of verification and validation processes to determine the accuracy of the developed FE model. Subsequently the discussions move into the failure modes of stiffened plates where the developed FE model was extended to incorporate difference stiffeners sizes and configurations. In this study, four different sizes of stiffeners, which represent four different width-to-height (*b/d*) ratios as tabulated in Table 2, were used where each size consist of four difference stiffeners configurations as depicted in Fig. 2.

Verification and Validation of FE Model

Prior to the actual study, the FE model of unstiffened steel plates was assessed through verification and validation process for the accuracy of the FE model. The FE model was verified via a mesh sensitivity study in which the maximum displacement of the plate was the measured parameter. In general, the FE model could be said to be insensitive to the mesh or number of elements when the observed parameter become constant, or the change of the observed parameter is very small when the mesh become finer. For this study, only the size of the element of the plate was changed while the mesh of the bolts and clamps were constant for all tests. From the tests, it was decided to use average element size of 0.5 mm for validation of the FE model. The reason for this was that the difference in the maximum displacement of the plate between Mesh 5 and Mesh 6 is only 3.7% while the computational resources increased significantly. The CPU time clocked by Abaqus for Mesh 6 is 73% higher than the Mesh 5. Thus, the change in displacement and computational time is not balanced quite well. The results of the mesh sensitivity study are tabulated in Table 3 and illustrates in Fig. 3.

Table 2 Geometric properties of the stiffeners

Stiffener's size, breadth (b) × depth (d) (mm)	b/d ratio	Stiffener's second moment of area about major axis, I_{xx} (mm^4)	Stiffener's second moment of area about minor axis, I_{yy} (mm^4)
3 × 6	0.5	13.5	54.0
6 × 6	1.0	108.0	108.0
9 × 6	1.5	364.5	162.0
12 × 6	2.0	864.0	216.0

The validation of the FE model was performed on the unstiffened FE model. The FE model was validated against Series 1 test series of the experimental program conducted by Yuen et al. [34]. In Series 1, eight different PE4 charge mass was used in the range of 8–28 g while the standoff distance was constant at 40 mm.

Table 4 shows the experiment test data and numerical results. In general, the numerical results give a mixed result where in 4 cases the maximum displacements are lower than the experiment while 2 of them are slightly higher. The other two analyses indicate the torn of the steel plates as depicted in Fig. 4. The form or shape of the failure of the plate from the numerical analysis could not be compared side by side with the experimental observation because no figures were produced in the report by the authors. Nonetheless, based on the failure from the numerical analysis, it could be suggested they are similar with the test data based on the mode of failure. The results, therefore, could be considered as acceptable where the difference between experiment and FE is within 3% to 15%. This variation is lower compared to other numerical studies reported in literature where for example, Mehreganian

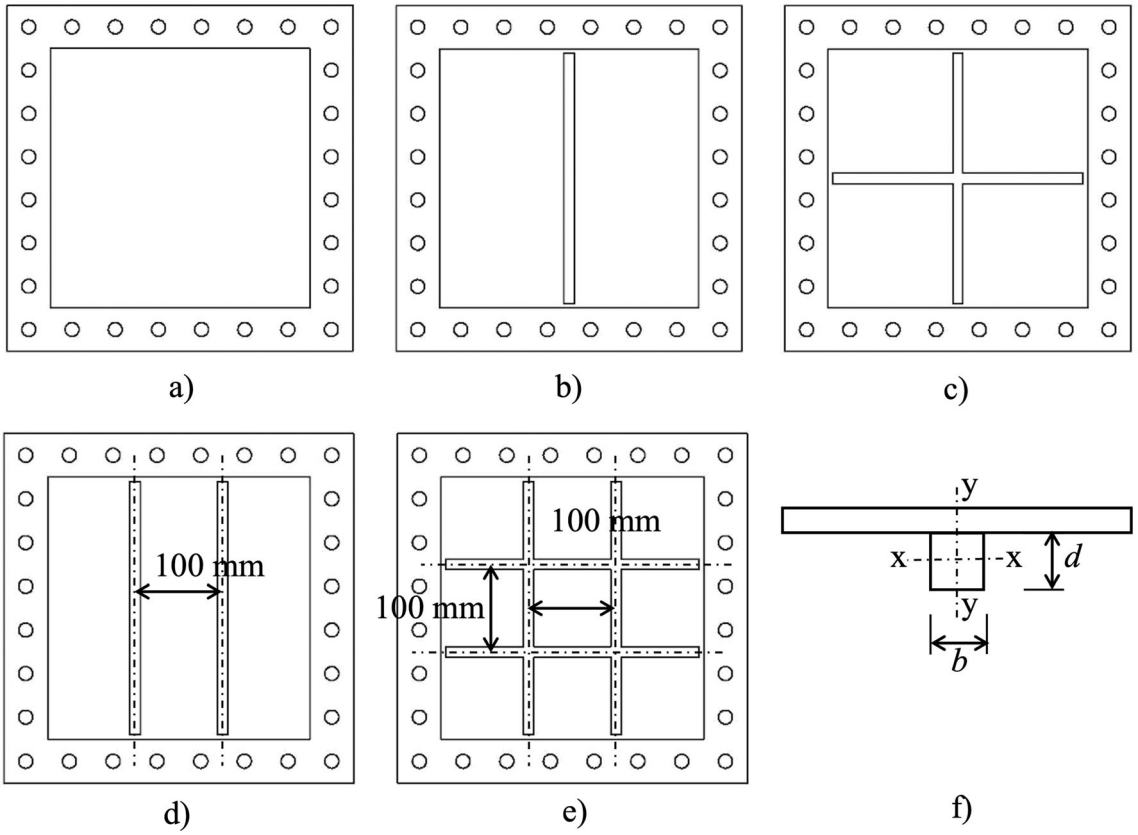

Fig. 2 Schematic drawings of (**a**) Unstiffened (control), (**b**) Single Stiffener (SS), (**c**) Cross Stiffener (CS), (**d**) Double Stiffener (DS), (**e**) Double-Cross Stiffener (DC) and (**e**) example of schematic side view drawing of stiffened steel plates with different b/d ratios

Table 3 Mesh sensitivity study of unstiffened steel plate

Specimen	Average element size of steel plate (mm)	Number of elements	Maximum displacement (mm)
Mesh 1	8	960	26.7
Mesh 2	4	5072	50.4
Mesh 3	2	15,232	52.0
Mesh 4	1	129,586	53.3
Mesh 5	0.5	1,067,280	54.3
Mesh 6	0.25	8,378,984	56.3

et al. [18] and Markose and Rao [51] showed that their numerical models overestimate the results by almost 30%, while Gan et al. [10] reported the error up to 20%. Thus, it could be concluded the developed FE model is sufficiently reliable and can be extended for further study.

Numerical Observations of Stiffened Plates

For the study of stiffened steel plates, only three blast loads, namely P5, P6 and P7, were selected from eight blast loads as tabulated in Table 4. These blast loads were selected because these are the loads where the mode of failure of the unstiffened plates changed from permanent displacement to tearing of plates as observed in experiment and numerical observations as discussed in previous section. Therefore, the results of unstiffened steel plate P5, P6 and P7 were taken as control specimens and redesignated herein as Ctrl-P5, Ctrl-P6 and Ctrl-P7, respectively. The summary of the numerical results from FE analyses is summarized in Table 5. This section discusses the general response and mode of failure of stiffened steel plates based on the numerical analyses.

Single Stiffener Series (SS)

The numerical analysis of the SS series suggested all the plates failed due to the plate tearing at the plate-stiffener edge. In general, the plate tearing started at the central area of the plate before progressively expended or move along the edge of stiffener. The length of the tearing of the plate was increased when the blast loads were increased. The increase in tearing's length can be observed from Fig. 5a, b and c. It was observed as well that two plates, SS-0.5-P6 and SS-0.5-P7, exhibited the rupture of stiffeners following tearing of the plate at plate-stiffener edge. The plate

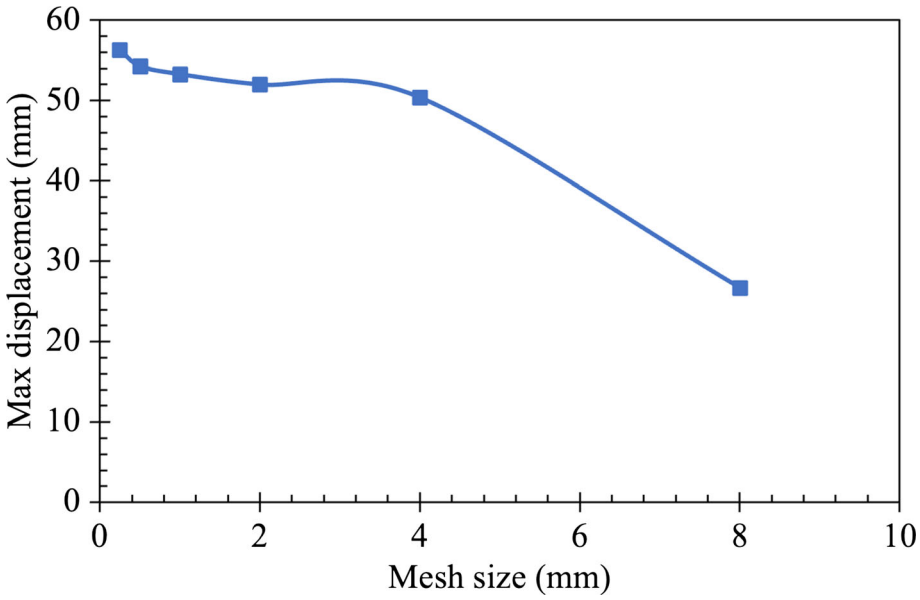

Fig. 3 The influence of mesh sizes on the maximum displacement of unstiffened steel plates

Table 4 Comparison between experiment and finite element results

Blast ID	PE4 (g)	TNT_{eqv} (g)	Maximum displacement, (mm)		FE/Exp (%)	Mode of failure
			Experiment [34]	FE analysis		
P1	8	14.6	22.1	21.3	− 3.6	Mode I
P2	10	18.2	28.3	25.5	− 9.9	Mode I
P3	12	21.9	33.3	32.2	− 3.3	Mode I
P4	14	25.5	37.1	38.3	3.2	Mode I
P5	16	29.1	40.0	45.8	14.5	Mode I
P6	18	32.8	44.5	49.6	11.4	Mode I
P7	20	36.4	Torn	Torn	Torn	Mode IIc
P8	28	51.0	Torn	Torn	Torn	P

MI: Mode I (Plastic deformation), MIIc: Mode IIc (complete tearing at central area: capping), P: petalling

ruptured at the centre of the plate and as the analysis progresses the plate folded outward excessively and broken away from the plate became a projectile as depicted in Fig. 6. As the stiffener size was increased, the plate only exhibited plate tearing at the stiffener edge and the length of the torn plate reduces. No rupture of stiffeners was observed as depicted in Fig. 5d, e and f. However, the SS series was found to fail at a much lower blast impulse compared to the control plates when subjected to P5, P6 and P7 blast pressures.

Cross Stiffener Series (CS)

The CS series exhibited a better performance compared to the SS series control series. Firstly, the onset of failure of the plate occurred when the plate was subjected to P6 blast load compared to the SS series. On the other hand, the maximum central displacement of CS-0.5-P5 and CS-0.5-P6 is lower compared to the control series, Ctrl-P5 and Ctrl-P7 as summarized in Table 5. However, the CS series presented with lower failure blast impulse compared to the control series, but slightly higher blast failure threshold compared to SS series. The observed modes of failure in CS series are inelastic plastic deformation, partial tearing of plate at the plate-stiffener edge or a combination of both modes as manifested in CS-0.5-P6 and CS-1.0-P7 as presented in Fig. 7. It was observed that the maximum displacement of CS series reduces as the size of stiffeners increases and the mode of failure change from partial tearing to permanent plastic deformation.

Double Stiffener Series (DS)

The DC series exhibited mainly tearing of steel plates at the central area where the impact of blast is the highest except for DS-2.0-P5. The plate failed due to the tearing of the plate the central area and the tearing line propagates towards the stiffener. The stiffener restrained the tearing line form propagates beyond the stiffener line and because of the it moved along the plate-stiffener edge and caused the plate to folded creating 'petals'. Like the SS and CS series, the stiffened plate failed at much lower blast impulse and the torn area increases as the blast impulse increases and this progression can be observed from Fig. 8a, b and c. It was observed from Fig. 8c, d, e and f that the torn area increases as the size of the stiffeners increases and this observation is also manifested in term of the damage energy predicted from the numerical analyses as depicted in Fig. 9.

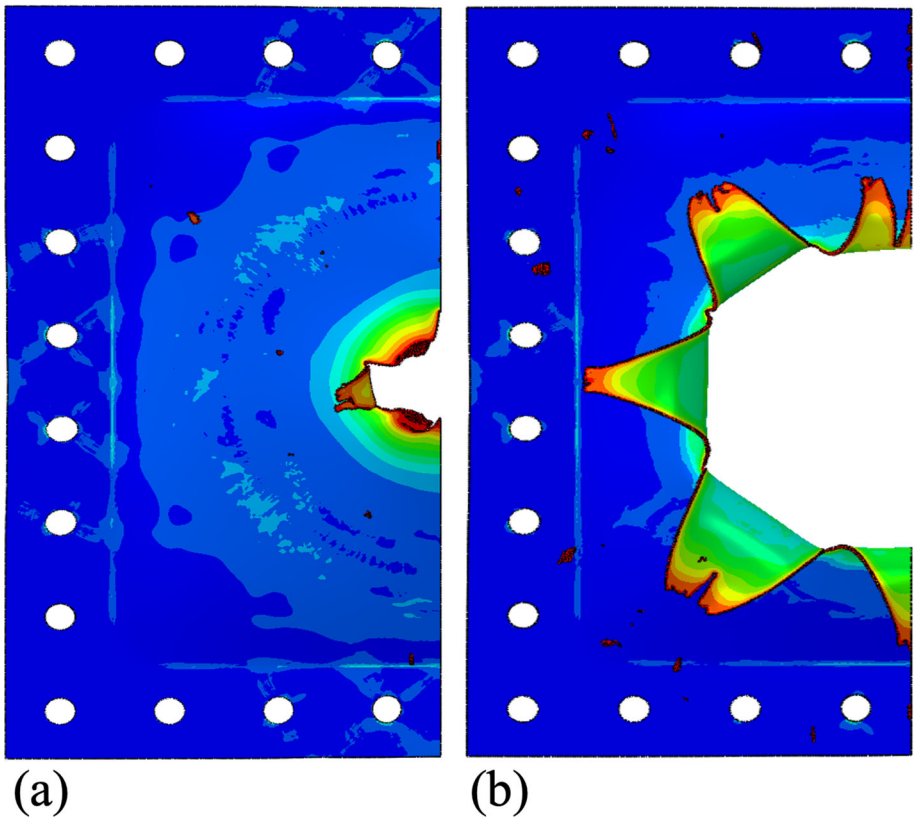

Fig. 4 The predicted failure of unstiffened steel plates subjected to (**a**) 36.4 g and (**b**) 51.0 g of TNT from the numerical simulations

Double Cross Stiffener Series (DC)

The response and mode of failure DC series are more or less like the DS series even though the DC series has more stiffeners around the central area of the plate. The influence of a greater number of stiffeners does not significantly affect the response. For example, the maximum displacement of DS-0.5-P5 plate compared to DS-0.5-P5 plate reduces only by 1.1%. The damage energy of the DC series as depicted in Fig. 10 suggests that increasing the number of stiffeners around the central area of the impact increases the damage of the steel plate. Thus, it implies that increasing the rigidity of the plate may only causes the plate presented with more severe damage or failure. This observation is evident from the change of the area of the failed plate as predicted from the numerical results presented in Fig. 11c, d, e and f.

The Influence of Stiffeners on Modes of Failure

Langdon et al. [4] has reported that stiffened steel plates tend to fail, specifically tearing of the plate, at lower blast impulse when compared to unstiffened plates. This section was aimed to investigate if a similar finding could be found or observed in this study. To investigate this behaviour, the charge weight in used were P5, P6 and P7 as these were the charge weight at the boundary or transition of mode of failure from Mode I, permanent plastic deformation, to Mode II, which is beam/plate tearing and petalling [2]. Petalling occurs when the torn plate folded outward. The Mode II failure is divided into different sub-failure modes based on the numerical observation. Two new sub-failure are proposed which are Mode II*s to represent the failure of plate along stiffener edge, and Mode IIs is assigned when the stiffener is ruptured. This proposed mode of failure are based on the numerical observation as summarised in Table 5. Another sub-failure mode is Mode IIc is for capping failure which when the plate is torn complete are central area and the last mode of failure is to Jacob et al. [2]. This study was performed on different stiffeners configurations but with a similar *b/d* ratio, which was 0.5.

The modes of failure of unstiffened (control) and stiffened steel plates are tabulated in Table 6. For the control plates, the tearing of the plate occurred at blast load P7. On the other hand, all stiffened steel plates torn at a lower blast load, which is at P6 except for CS-0.5 plates. Therefore, the results from this numerical study concur with the finding of Langdon et al. [4]. The CS-0.5 plates indicated obvious tearing of plate along the stiffener with rupture of stiffener when the plate was subjected to P7 blast load as depicted in Fig. 12. The tearing of the plate was found to be folded outward, and this deformation is known to be as 'petalling'

Table 5 Summary of near-field blast simulations of unstiffened (control) and stiffened steel plates

Specimen						
Type	Stiffener size (mm)	Plate ID	TNT mass (g)	Reflected pressure (MPa)	Mid disp (mm)	Observations
Unstiffened (control)	N/A	Ctrl-P5	29.1	275.4	45.8	Permanent plastic deformation
	N/A	Ctrl-P6	32.8	289.1	49.6	Permanent plastic deformation
	N/A	Ctrl-P7	36.4	300.6	…	Tearing of plate at central area
Single stiffener (SS)	3 × 6	SS-0.5-P5	29.1	275.4	…	Partial tearing of plate along stiffener edge
	3 × 6	SS-0.5-P6	32.8	289.1	…	Partial tearing of plate along stiffener edge and rupture of stiffener
	3 × 6	SS-0.5-P7	36.4	300.6	…	Partial tearing of plate along stiffener edge and rupture of stiffener
	6 × 6	SS-1.0-P7	36.4	300.6	…	Partial tearing of plate along stiffener edge and rupture of stiffener
	9 × 6	SS-1.5-P7	36.4	300.6	…	Partial tearing of plate along stiffener edge
	12 × 6	SS-2.0-P7	36.4	300.6	…	Partial tearing of plate along stiffener edge
Cross stiffener (CS)	3 × 6	CS-0.5-P5	29.1	275.4	37.8	Permanent plastic deformation
	3 × 6	CS-0.5-P6	32.8	289.1	42.5	Permanent plastic deformation
	3 × 6	CS-0.5-P7	36.4	300.6	…	Partial tearing of plate along stiffener edge and rupture of stiffener
	6 × 6	CS-1.0-P7	36.4	300.6	43.6	Permanent plastic deformation and partial tearing of plate along stiffener edge
	9 × 6	CS-1.5-P7	36.4	300.6	38.3	Permanent plastic deformation
	12 × 6	CS-2.0-P7	36.4	300.6	37.0	Permanent plastic deformation
Double stiffener (DS)	3 × 6	DS-0.5-P5	29.1	275.4	43.7	Permanent plastic deformation
	3 × 6	DS-0.5-P6	32.8	289.1	…	Tearing of plate at central area
	3 × 6	DS-0.5-P7	36.4	300.6	…	Petalling
	6 × 6	DS-1.0-P7	36.4	300.6	…	Petalling
	9 × 6	DS-1.5-P7	36.4	300.6	…	Petalling
	12 × 6	DS-2.0-P7	36.4	300.6	…	Tearing of plate along stiffener edge and petalling
Double cross stiffener (DC)	3 × 6	DC-0.5-P5	29.1	275.4	43.2	Permanent plastic deformation
	3 × 6	DC-0.5-P6	32.8	289.1	…	Tearing of plate at central area
	3 × 6	DC-0.5-P7	36.4	300.6	…	Petalling
	6 × 6	DC-1.0-P7	36.4	300.6	…	Petalling
	9 × 6	DC-1.5-P7	36.4	300.6	…	Petalling
	12 × 6	DC-2.0-P7	36.4	300.6	…	Tearing of plate along stiffener edge and petalling

[4]. At P6, however, it was found that there is a slight damage to the plate based on the predicted damage energy from the numerical simulation as shown in Fig. 13. The damage, however, does not materialised into tearing of the plate. Therefore, the failure model of the CS-0.5-P6 plate is considered as Mode 1. The numerical results suggest SS-0.5 plates seem to be more prone to tearing as the plate torn at P5 compared to other stiffener configurations. The tearing of plate, in general, starts from the centre to the plate and propagates towards or along the plate-stiffeners junction.

The failure of stiffened steel plates at lower blast loads could be contributed by the stress–strain concentration at the plate-stiffener edge is because of abrupt change of cross-section of the plate due to the presence of the stiffener. The change of cross-section has created a sharp corner or right angle at the plate-stiffener edge. It is well known that any right angle would create concentration of stress and strain at a corner [37]. This phenomenon could be observed more clearly from the deformation phase of SS plate as shown in Fig. 14. As the plate continuously in motion and deforms, the stress and strain increase at the corner and as the strain reached its fracture strain the elements that representing the plate are deleted indicating the nucleation of void and the void growth and coalesces with other voids to form fractures.

The numerical results suggest the stiffeners act like a restraint or support to the plate, which depending on the location of the stiffeners, it affects the deformation shape of the plate at early stage of the motion as shown in Fig. 15. While most steel plates indicate the maximum displacement occur at the centre of the plate, the SS plate

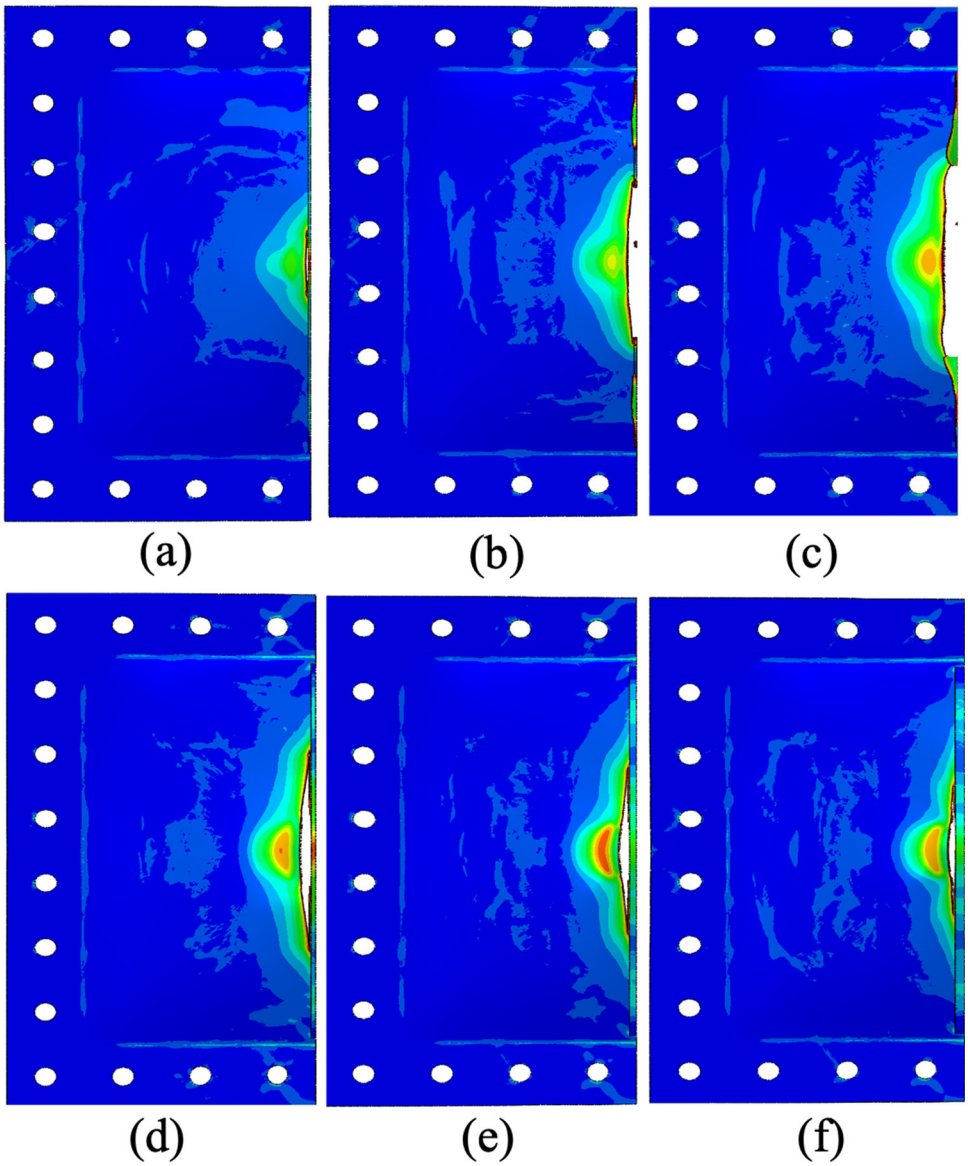

Fig. 5 FE predictions of the response of (**a**) SS-0.5-P5, (**b**) SS-0.5-P6, (**c**) SS-0.5-P7, (**d**) SS-1.0-P7, (**e**) SS-1.5-P7 and (**f**) SS-2.0-P7 stiffened steel plates

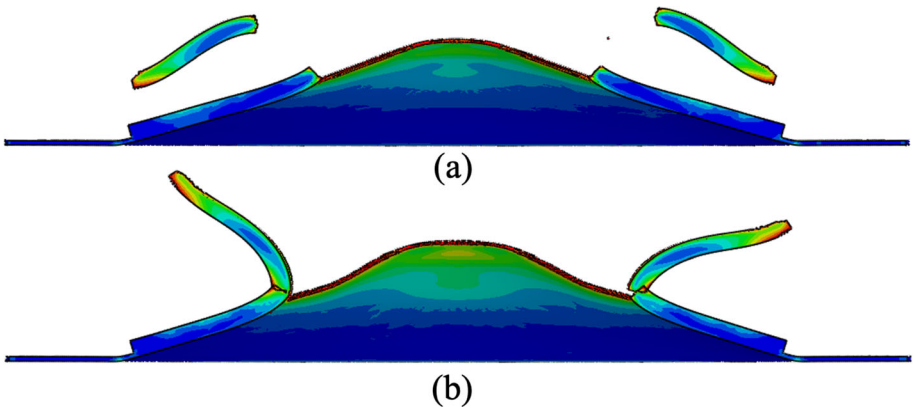

Fig. 6 The rupture of stiffeners in (**a**) SS-0.5-P6 and (**b**) SS-0.5-P7

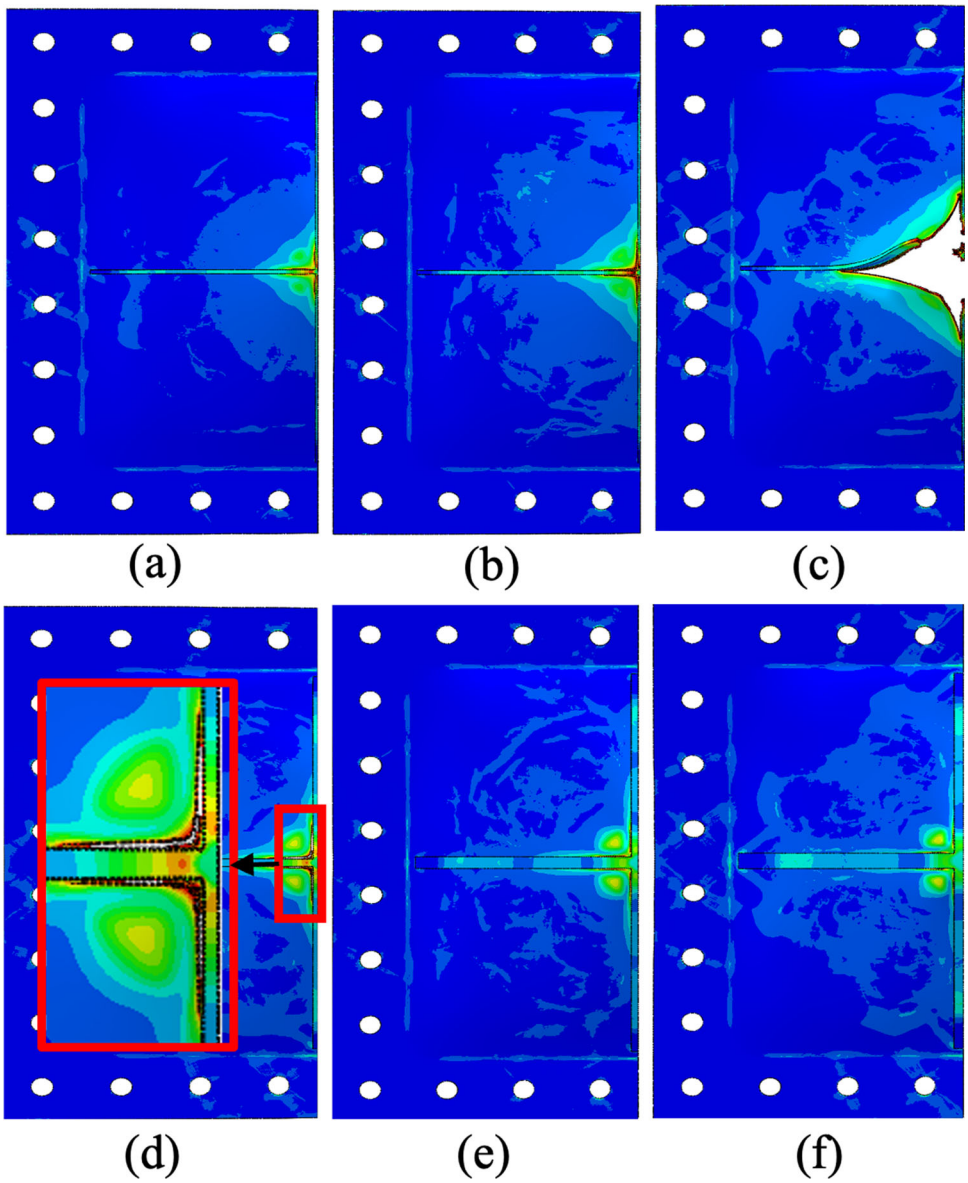

Fig. 7 FE predictions of the response of (**a**) CS-0.5-P5, (**b**) CS-0.5-P6, (**c**) CS-0.5-P7, (**d**) CS-1.0-P7, (**e**) CS-1.5-P7 and (**f**) CS-2.0-P7 stiffened steel plates

shows on the contrary. For SS plate, the peak of the plate profile at early state of motion occurs in the unstiffened area of the plate near to the stiffener as depicted in Fig. 15. It is also interesting to note that although stiffeners are presence in DS and DC plates, the deformation of the plate at the central area at early stage is like the control plate. Although the deflection profiles are similar, different results are obtained from the numerical analysis. The analysis indicates DS and DC plates failed due to plate tearing (Mode II) while the control plate sustains permanent plastic deformation (Mode I). This difference could be contributed by the stiffeners as it can be seen from the inset in Fig. 15 there is a slightly different to the deformation profiles of DS and DC plates compared to the control (CTRL) plate in which suggest the CTRL plate is slightly flexible compared to the DS and DC plates at the point. This flexibility could allow the CTRL plate to dissipate the plastic energy slightly higher in the form of bending mechanism compared to DS and DC plate. Figure 16 shows the comparison of the plastic dissipation energy of the plates in Table 6 for comparison especially for P6 blast load cases where all the stiffened plates failed due to the fracture of the plate.

The Effect of the Sizes of the Stiffeners

In structural analysis and design, it is quite common to postulate that larger section or larger number of section is better in providing structural resistance. With the same idea, this study increases the size the stiffeners to

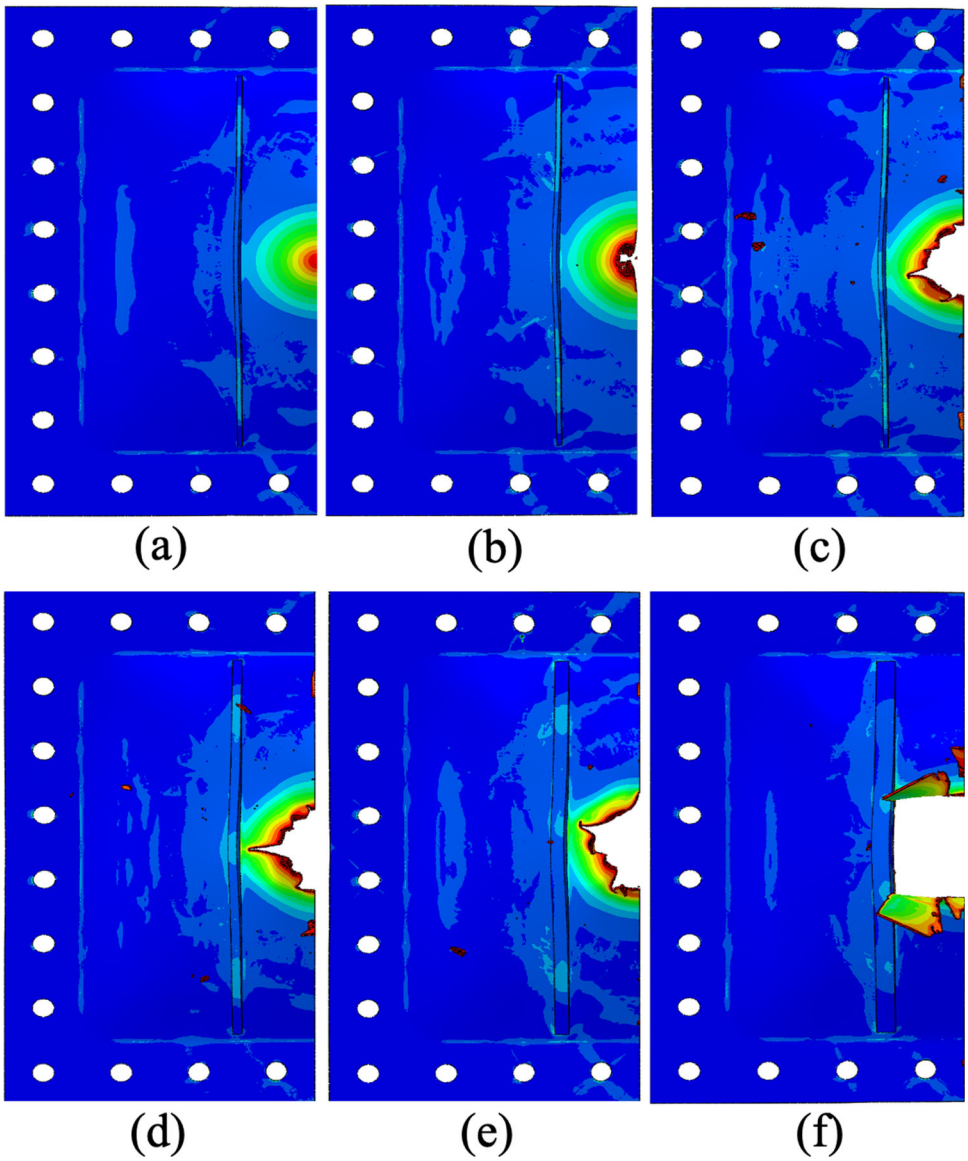

Fig. 8 FE predictions of the response of (**a**) DS-0.5-P5, (**b**) DS-0.5-P6, (**c**) DS-0.5-P7, (**d**) DS-1.0-P7, (**e**) DS-1.5-P7 and (**f**) DS-2.0-P7 stiffened steel plates

investigate the stiffened plates behaviour in particular the failure of the plates and this setting was tested in four different stiffeners configurations. The modes of failure of stiffened plates with different *b/d* ratio and stiffener configurations are tabulated in Table 7 where all plates were subjected to the same blast pressure of 36.4 g of TNT (P7).

The investigation reveals that increasing the size of the stiffeners could reduce and increase the failure of the steel plates at the same time. Figure 17 shows the damage energy of all stiffened steel plates where it can be observed that for SS and CS plates the damage energy reduces as the *b/d* ratio increases. This phenomenon also could be observed from the failure of SS and CS plates in Fig. 18a and b where the torn area reduces as the *b/d* ratio increases. Hence, it is evidence increasing the size of stiffeners reduces the deformation of the plate and the damage become less severe. The mode of failure also could change from tearing type failure (Mode II) to permanent deformation as in CS plate series. This result could be contributed by the position of the stiffeners in both plates, SS and CS plate, where the stiffeners are positioned at the point of the highest blast pressure. Because of the position of the stiffeners, the second moment of area of the plates cross-section at the specific point of impact has increased. This increment means the bending resistance of the increases, hence, reduces the deformation of the plates.

The results from DS and DC plates, on the other hand, suggest that the increase of stiffeners size does not improve the deformation and failure of these plates. Their damage energy suggests the damage of the plate become more severe when the size of stiffeners increases as depicted in Fig. 17. The damage energy increases as the *b/d* ratio

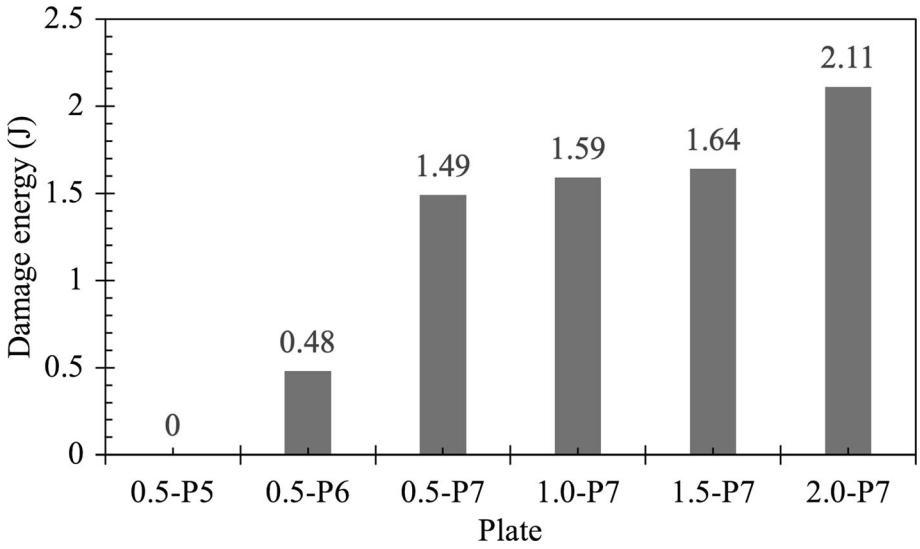

Fig. 9 Damage energy of doubly stiffened steel plates (DS series)

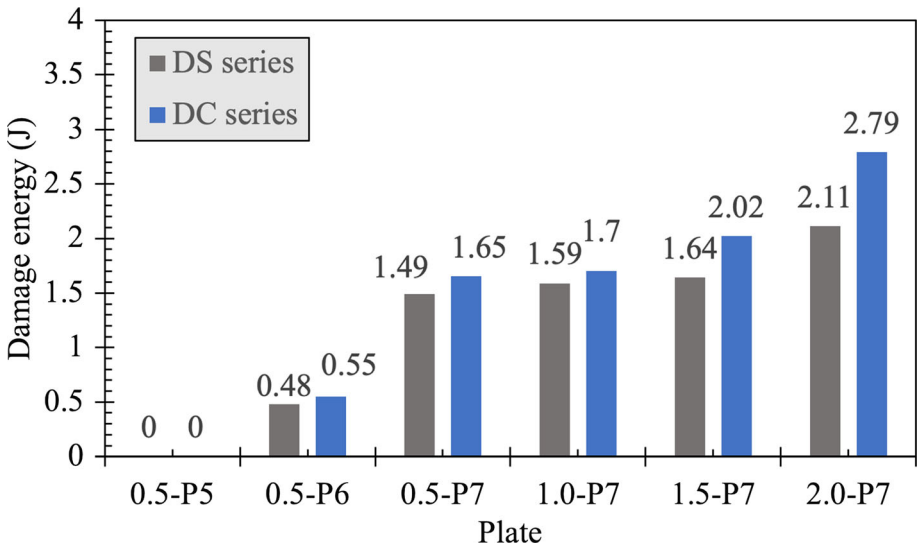

Fig. 10 Comparison of damage energy predicted from numerical analyses for DS and DC series of stiffened steel plates

increases, and this increment is translated into the damage of DS and DC plates as shown in Fig. 18c and d. It should be noted, however, that the stiffeners for DS and DC plates are at a distance from the point of the highest blast pressure. As a result, the second moment of inertia of the plates at the point impact for DS and DC series is like the control steel plate. Hence, this could be one of the contributing factors to the findings of DS and DC plates.

Another factor that could cause the damage in DS and DC plates more severe is because there are more and larger damaged area than that of SS and CS plates. The additional fracture areas in DS and DC plates are at the plate-stiffener edges which where plastic hinges form and expends as the plates continue to deform. The stress and strain at the plastic hinges continue to increase with the increase of plate deformation and at the end the strain reaches the fracture strain which cause the material or element to tear and damages the plate. Figure 19 shows the evolution of damage in unstiffened and stiffened (b/d = 2.0) plates where at t = 0.07 ms, plastic hinges formed at the plate-stiffener intersection and at t = 0.25 ms the plastic hinges has changed to fracture. As for the DC plates, there are four

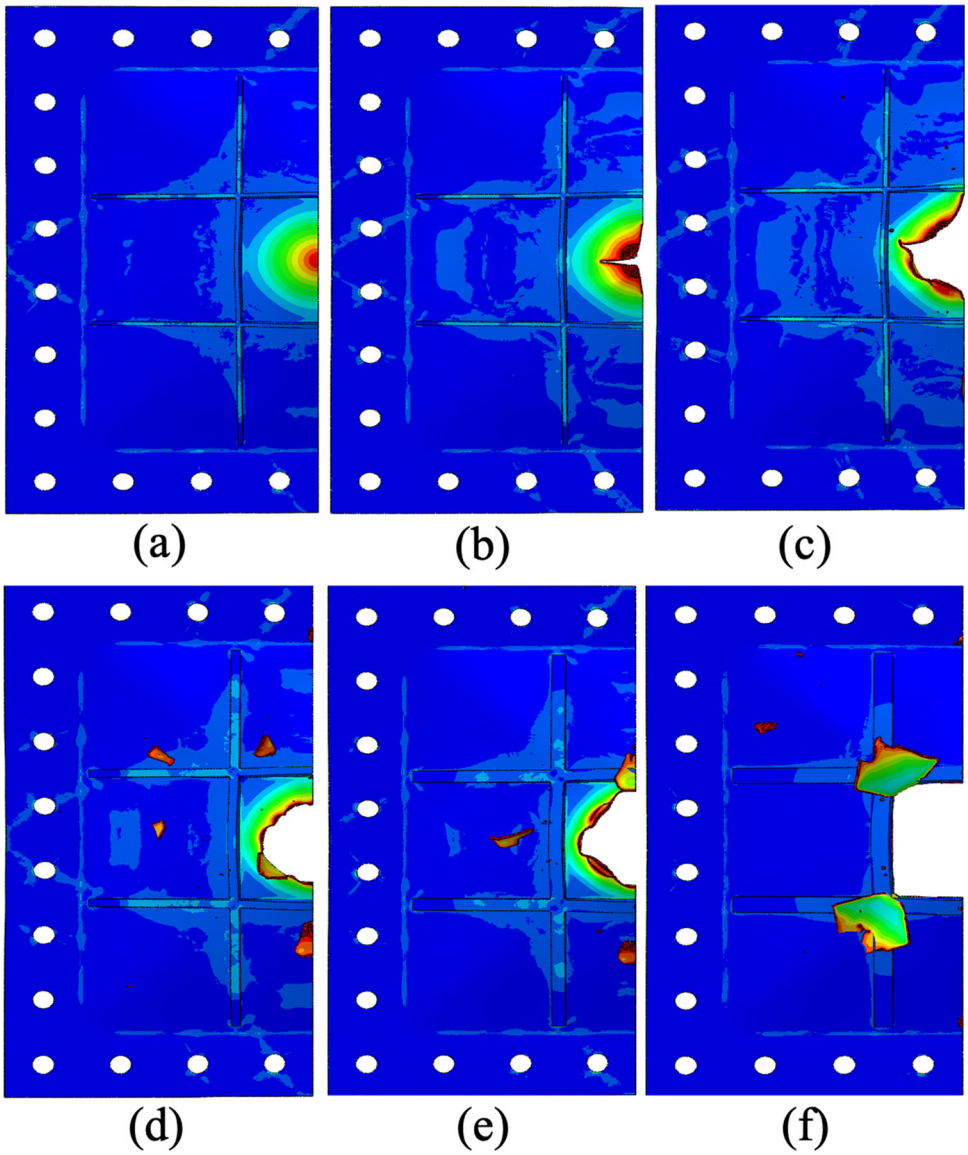

Fig. 11 FE predictions of the response of (**a**) DC-0.5-P5, (**b**) DC-0.5-P6, (**c**) DC-0.5-P7, (**d**) DC-1.0-P7, (**e**) DC-1.5-P7 and (**f**) DC-2.0-P7 stiffened steel plates

Table 6 The influence of stiffeners to the modes of failure of stiffened steel plates

			Stiffener series			
Blast ID	TNT (g)	Control	SS-0.5	CS-0.5	DS-0.5	DC-0.5
P5	29.1	MI	MII*s	MI	MI	MI
P6	32.8	MI	MII*s + MIIs	MI + MII*s	MIIc	MIIc
P7	36.4	MIIc	MII*s + MIIs	MII*s + MIIs	MIIc	P

MI: Mode I (Plastic deformation), MII*s: Mode II*s (Partial plate tearing along stiffener), MIIs: modeIIs (Rupture of stiffener), MIIc Mode: IIc (Complete plate tearing at central area: capping), P: petalling

plastic hinges (considering symmetrical condition) compared to two for the DS plates; thus, the DC plates sustain more fracture area in which increases the damage energy.

Conclusion

A numerical study on the failure of stiffened steel plates subjected to near-filed air blast load is reported herein. The FE model was initially develop for unstiffened steel plates according to the experimental program conducted by Yuen et al. [34]. The developed FE model was verified and validated against test data from reference [34]. The developed finite element model shows a good accuracy

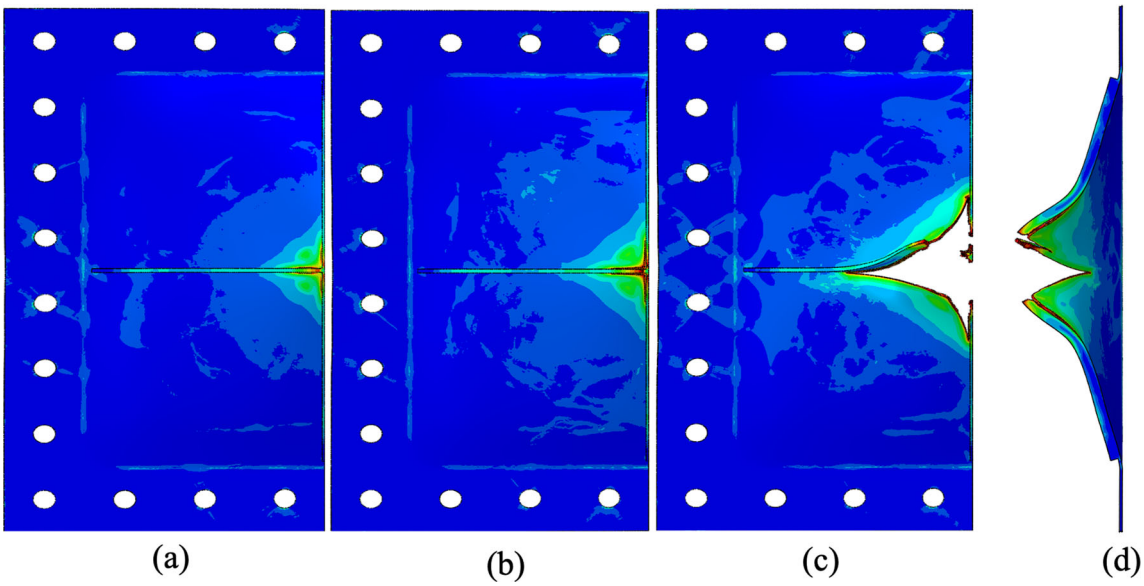

Fig. 12 The mode of failure of CS-0.5 steel plates subjected to (**a**) 29.1 g, (**b**) 32.8 g (**c**) 36.4 g of TNT and (**d**) is the rupture of stiffener of CS-05-P7 plate from side view

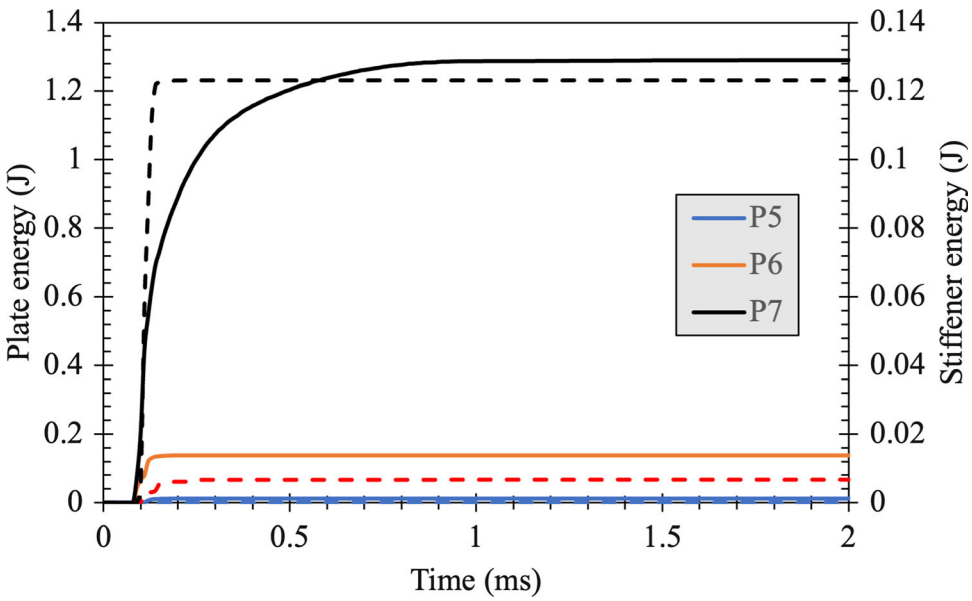

Fig. 13 Damage energy of plate (—— solid lines) and stiffener (- - - - dashed lines) of CS-0.5 stiffener plates subjected to blast loads

level against the experimental data. The developed FE model then was extended to incorporate stiffeners with different sizes and configurations, while other setting was maintained.

This numerical study has established that failure of stiffened steel plates could occur at much lower blast pressure when compared to unstiffened steel plate except for plate with cross stiffener configuration. The cross stiffener configuration has more resistance due to the position of the stiffener with respect to the point of the largest pulse acted.

Increasing the numbers or the sizes of the stiffeners could reduce and increase the severity of the failure of the stiffened steel plates. This behaviour is influenced by the point of high blast pressure with respect to the number and arrangement of the stiffeners. For stiffeners that positioned exactly at the point of impact, increasing the size of the stiffeners will reduce the damage or eliminate the failure of the stiffener steel plates. On the other hand, the damage or failure of stiffened steel plates could increase or become more severe when the stiffeners are position away from the point of impact even more than one number of stiffeners presence on the steel plates.

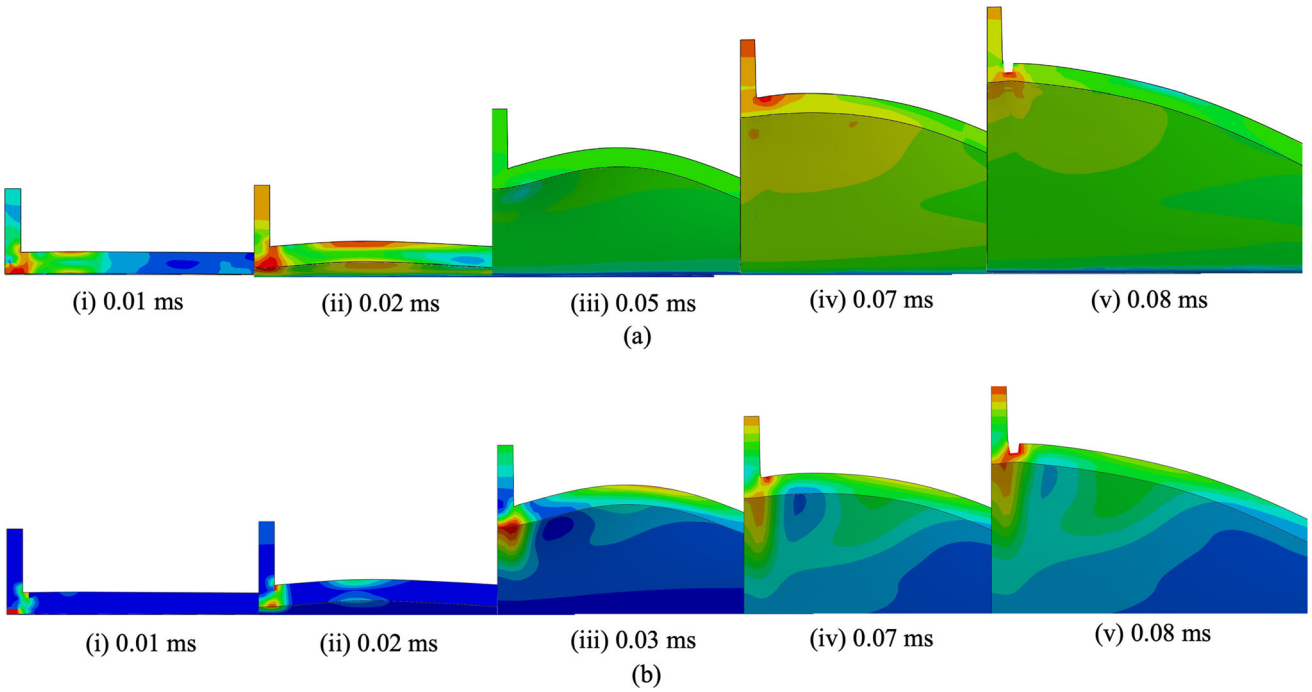

Fig. 14 Concentration of (**a**) stress and (**b**) strain at different stages of deformation in the early phase of motion of the plate around the plate-stiffener edge in SS-05-P6 plate

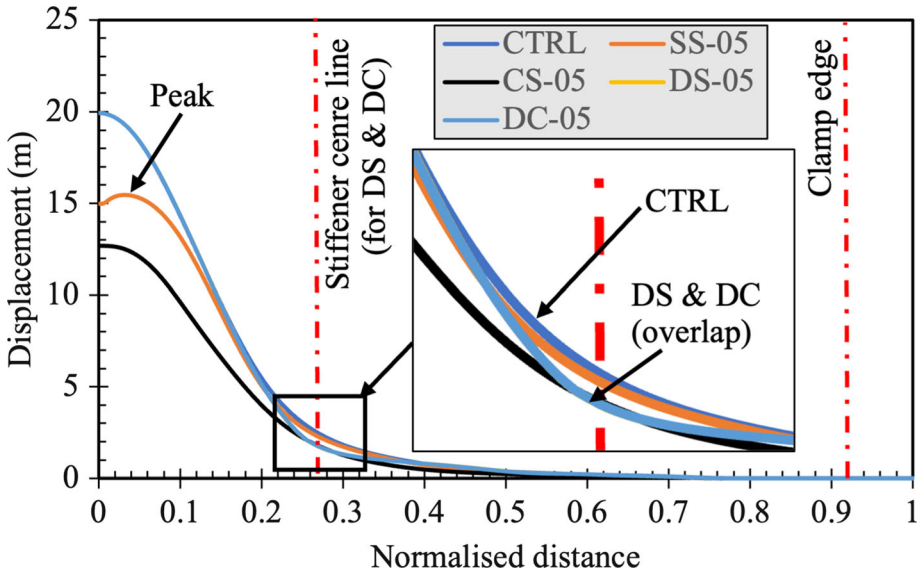

Fig. 15 Deformation profiles of steel plates subjected to P6 blast load at t = 0.05 ms

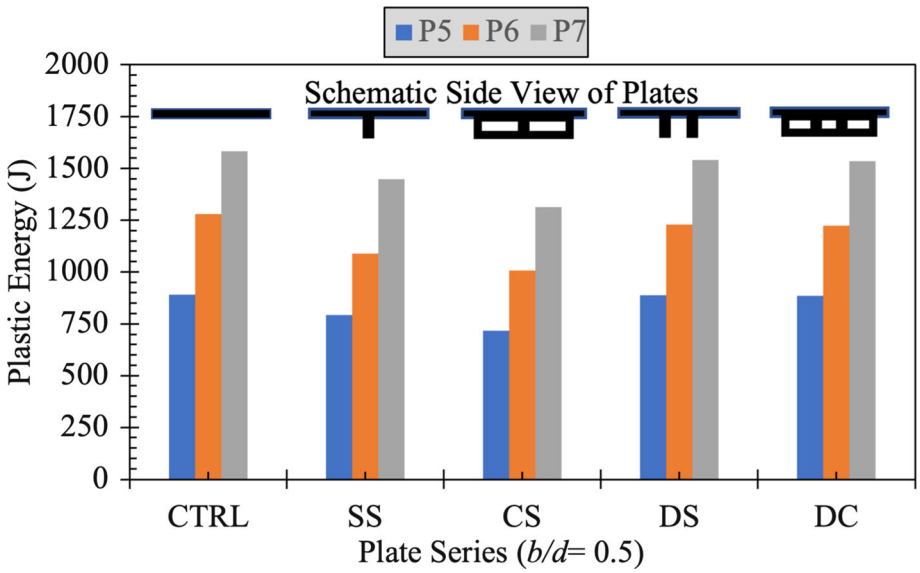

Fig. 16 Plastic dissipation energy of control and stiffened steel plates

Table 7 The influence of stiffeners width/height ratio and configurations to the modes of failure

			Stiffener series			
Blast ID	TNT (g)	*b/d*	SS	CS	DS	DC
P7	36.4	0.5	MII*s + MIIs	MII*s + MIIs	MIIc	P
		1.0	MII*s	MII*s + MI	MIIc	P
		1.5	MII*s	MI	P	P
		2.0	MII*s	MI	MII*s + P	MII*s + P

MI: Mode I (Plastic deformation), MII*s: Mode II*s (Partial plate tearing along stiffener), MIIs: ModeIIs (Rupture of stiffener), MIIc: Mode IIc (Complete plate tearing at central area: capping), P: petalling

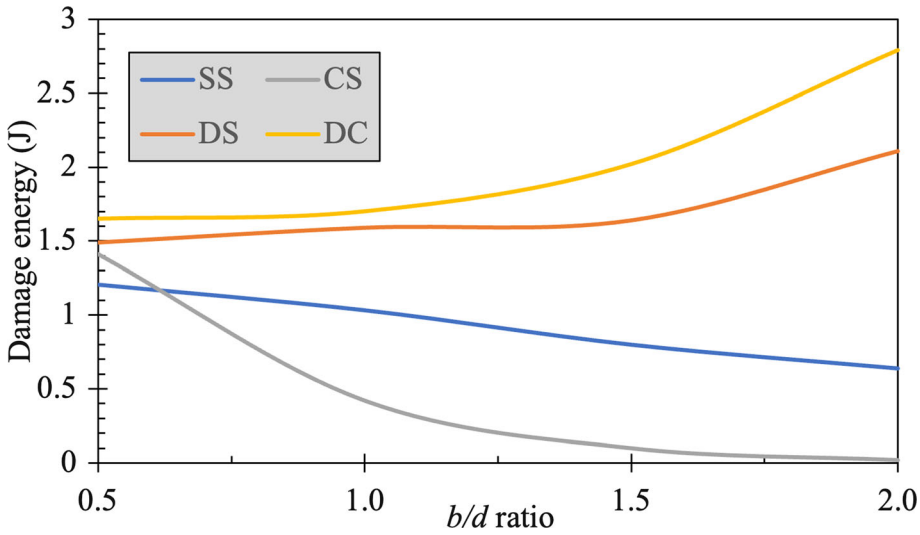

Fig. 17 Damage energy predicted from numerical simulations for stiffened steel plates with different stiffeners sizes and configurations subjected to 36.4 g of TNT

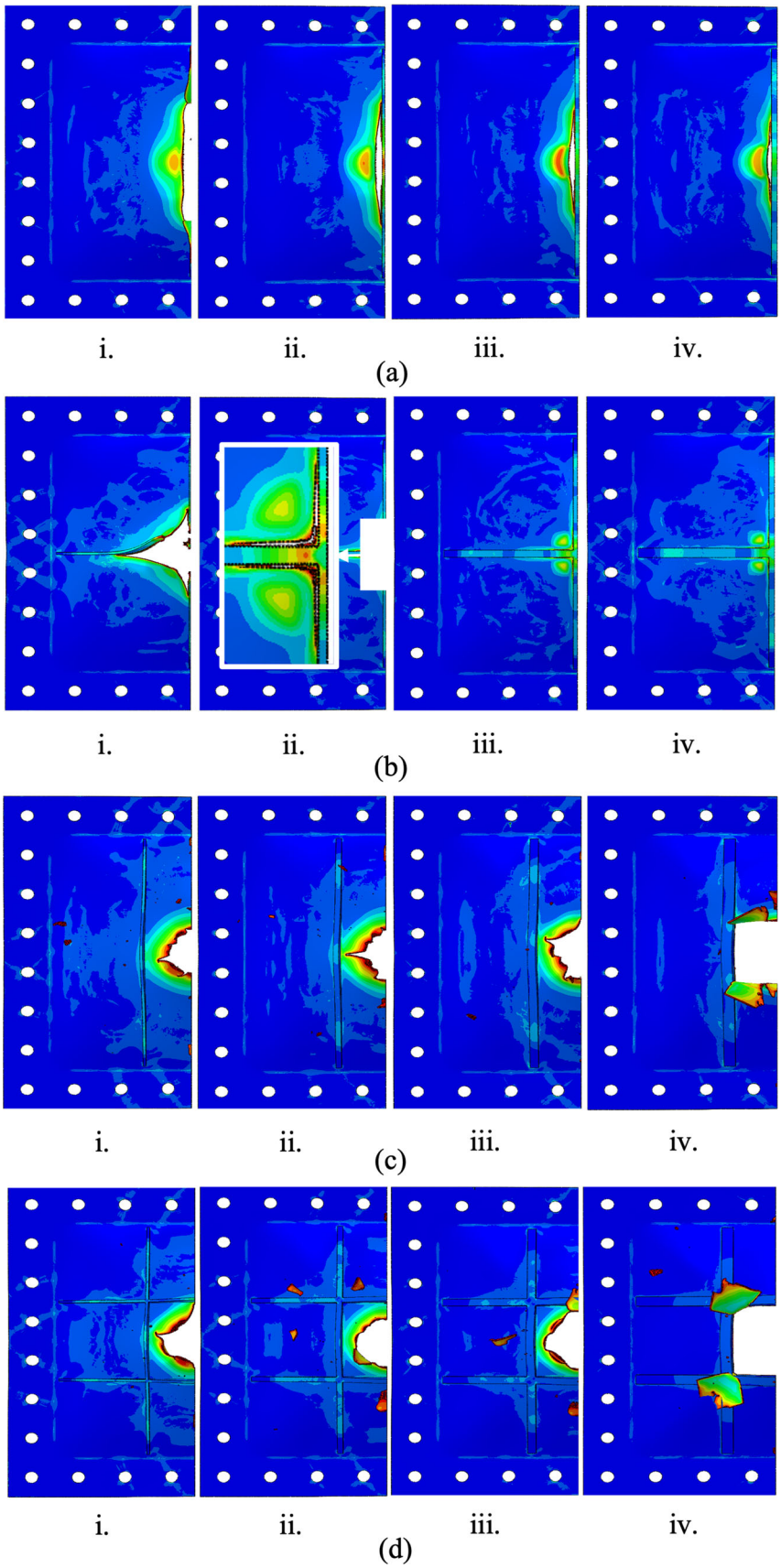

Fig. 18 The failure of (**a**) SS, (**b**) CS, (**c**) DS and (**d**) DC stiffened steel plates subjected to blast load of 36.4 g of TNT with different *b/d* ratios (i) 0.5, (ii) 1.0, (iii) 1.5 and (iv) 2.0

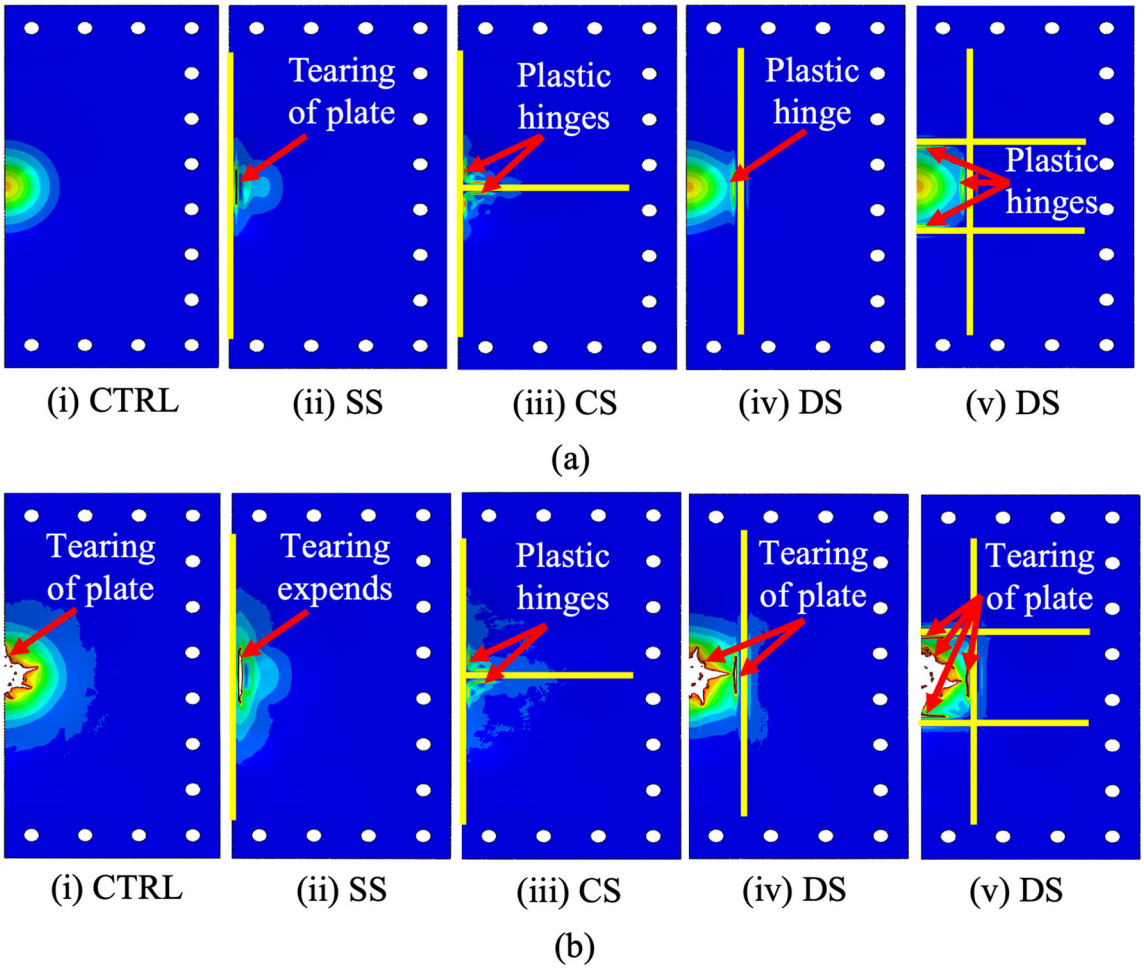

Fig. 19 The formation of plastic hinges and fracture of plates at (**a**) 0.07 ms and (**b**) 0.25 ms in unstiffened and stiffened steel plates subjected to P7 blast load

According to the numerical results, two new sub-modes of failure are proposed namely Mode II*s for partial plate tearing along stiffener and Mode IIs for rupture of stiffener.

Acknowledgments The authors would like to express their gratitude and thanks to UMP, UiTM and IIUM for funding this research under Sustainable Research Collaboration Grant (RDU200761).

References

1. S. Chung Kim Yuen, G.N. Nurick, G.S. Langdon, Y. Iyer, Deformation of thin plates subjected to impulsive load: Part III—an update 25 years on. Int. J. Impact Eng. **107**, 108–117 (2017). https://doi.org/10.1016/j.ijimpeng.2016.06.010
2. N. Jacob, G.N. Nurick, G.S. Langdon, The effect of stand-off distance on the failure of fully clamped circular mild steel plates subjected to blast loads. Eng. Struct. **29**(10), 2723–2736 (2007). https://doi.org/10.1016/j.engstruct.2007.01.021
3. S.C.K. Yuen, G.N. Nurick, Experimental and numerical studies on the response of quadrangular stiffened plates. Part I: subjected to uniform blast load. Int. J. Impact Eng. **31**(1), 55–83 (2005). https://doi.org/10.1016/j.ijimpeng.2003.09.048
4. G.S. Langdon, S.C.K. Yuen, G.N. Nurick, Experimental and numerical studies on the response of quadrangular stiffened plates. Part II: localised blast loading. Int. J. Impact Eng. **31**(1), 85–111 (2005). https://doi.org/10.1016/j.ijimpeng.2003.09.050
5. D. Bonorchis, G.N. Nurick, The influence of boundary conditions on the loading of rectangular plates subjected to localised blast loading: importance in numerical simulations. Int. J. Impact Eng. **36**(1), 40–52 (2009). https://doi.org/10.1016/j.ijimpeng.2008.03.003
6. T.F. Henchie, S. Chung Kim Yuen, G.N. Nurick, N. Ranwaha, V.H. Balden, The response of circular plates to repeated uniform blast loads: an experimental and numerical study. Int. J. Impact Eng. **74**, 36–45 (2014). https://doi.org/10.1016/j.ijimpeng.2014.02.021
7. S.C.K. Yuen, G.S. Langdon, G.N. Nurick, E.G. Pickering, V.H. Balden, Response of V-shape plates to localised blast load: experiments and numerical simulation. Int. J. Impact Eng. **46**, 97–109 (2012). https://doi.org/10.1016/j.ijimpeng.2012.02.007
8. S.E. Rigby, C. Osborne, G.S. Langdon, S.B. Cooke, D.J. Pope, Spherical equivalence of cylindrical explosives: effect of charge shape on deflection of blast-loaded plates. Int. J. Impact Eng. **155**(November 2020), 103892 (2021). https://doi.org/10.1016/j.ijimpeng.2021.103892

9. N.S.A. Razak, A. Alias, The response of steel plates subjected to close-in blast loads. IOP Conf. Ser. Earth Environ. Sci. **682**(1), 012036 (2021). https://doi.org/10.1088/1755-1315/682/1/012036
10. L. Gan, Z. Zong, J. Lin, Y. Chen, M. Xia, L. Chen, Influence of U-shaped stiffeners on the blast-resistance performance of steel plates. J. Constr. Steel Res. **188**(November 2021), 107046 (2022). https://doi.org/10.1016/j.jcsr.2021.107046
11. X. Kong et al., Corrected method for scaling the dynamic response of stiffened plate subjected to blast load. Thin-Walled Struct. **159**(June 2019), 107214 (2021). https://doi.org/10.1016/j.tws.2020.107214
12. D. Bonorchis, G.N. Nurick, The analysis and simulation of welded stiffener plates subjected to localised blast loading. Int. J. Impact Eng. **37**(3), 260–273 (2010). https://doi.org/10.1016/j.ijimpeng.2009.08.004
13. Y. Li, X. Ren, T. Zhao, D. Xiao, K. Liu, D. Fang, Dynamic response of stiffened plate under internal blast: experimental and numerical investigation. Mar. Struct. **77**(August 2020), 102957 (2021). https://doi.org/10.1016/j.marstruc.2021.102957
14. A. Ghani Razaqpur, A. Tolba, E. Contestabile, Blast loading response of reinforced concrete panels reinforced with externally bonded GFRP laminates. Compos. Part B Eng. **38**(5–6), 535–546 (2007). https://doi.org/10.1016/j.compositesb.2006.06.016
15. V. Aune, G. Valsamos, F. Casadei, M. Langseth, T. Børvik, Fluid-structure interaction effects during the dynamic response of clamped thin steel plates exposed to blast loading. Int. J. Mech. Sci. **195**(December), 2021 (2020). https://doi.org/10.1016/j.ijmecsci.2020.106263
16. R.J. Curry, G.S. Langdon, Transient response of steel plates subjected to close proximity explosive detonations in air. Int. J. Impact Eng. **102**, 102–116 (2017). https://doi.org/10.1016/j.ijimpeng.2016.12.004
17. K. Micallef, A.S. Fallah, P.T. Curtis, L.A. Louca, On the dynamic plastic response of steel membranes subjected to localised blast loading. Int. J. Impact Eng. **89**, 25–37 (2016). https://doi.org/10.1016/j.ijimpeng.2015.11.002
18. N. Mehreganian, L.A. Louca, G.S. Langdon, R.J. Curry, N. Abdul-Karim, The response of mild steel and armour steel plates to localised air-blast loading-comparison of numerical modelling techniques. Int. J. Impact Eng. **115**(May 2017), 81–93 (2018). https://doi.org/10.1016/j.ijimpeng.2018.01.010
19. R.P. Bohara, S. Linforth, A. Ghazlan, T. Nguyen, A. Remennikov, T. Ngo, Performance of an auxetic honeycomb-core sandwich panel under close-in and far-field detonations of high explosive. Compos. Struct. **280**(February 2021), 114907 (2021). https://doi.org/10.1016/j.compstruct.2021.114907
20. B. Zakrisson, B. Wikman, H.-Å. Häggblad, Numerical simulations of blast loads and structural deformation from near-field explosions in air. Int. J. Impact Eng. **38**(7), 597–612 (2011). https://doi.org/10.1016/j.ijimpeng.2011.02.005
21. K. Micallef, A.S. Fallah, D.J. Pope, L.A. Louca, The dynamic performance of simply-supported rigid-plastic circular steel plates subjected to localised blast loading. Int. J. Mech. Sci. **65**(1), 177–191 (2012). https://doi.org/10.1016/j.ijmecsci.2012.10.001
22. N. Mehreganian, A.S. Fallah, L.A. Louca, Plastic dynamic response of simply supported thick square plates subject to localised blast loading. Int. J. Impact Eng. **126**(April 2018), 85–100 (2019). https://doi.org/10.1016/j.ijimpeng.2018.12.010
23. A.S. Fallah, L.A. Louca, Pressure-impulse diagrams for elastic plastic hardening and softening single degree of freedom models subjected to blast loading.pdf. Int. J. Impact Eng. **34**, 823–842 (2007)
24. G. Randers-Pehrson, K.A. Bannister, Airblast loading model for DYNA2D and DYNA3D (1997)
25. G.F. Kinnery, K.J. Graham, *Explosive Shocks in Air*. (Springer, Berlin, 1985)
26. S.E. Rigby, A. Tyas, T. Bennett, Single-Degree-of-Freedom response of finite targets subjected to blast loading: the influence of clearing. Eng. Struct. **45**, 396–404 (2012). https://doi.org/10.1016/j.engstruct.2012.06.034
27. L. Lomazzi, M. Giglio, A. Manes, Analytical and empirical methods for the characterisation of the permanent transverse displacement of quadrangular metal plates subjected to blast load: comparison of existing methods and development of a novel methodological approach. Int. J. Impact Eng. **154**(April), 103890 (2021). https://doi.org/10.1016/j.ijimpeng.2021.103890
28. J. Shin, A.S. Whittaker, D. Cormie, TNT equivalency for overpressure and impulse for detonations of spherical charges of high explosives. Int. J. Prot. Struct. **6**(3), 567–579 (2015). https://doi.org/10.1260/2041-4196.6.3.567
29. X. Lin, Y.X. Zhang, P.J. Hazell, Modelling the response of reinforced concrete panels under blast loading. Mater. Des. **56**, 620–628 (2014). https://doi.org/10.1016/j.matdes.2013.11.069
30. K.P. Dharmasena, H.N.G. Wadley, Z. Xue, J.W. Hutchinson, Mechanical response of metallic honeycomb sandwich panel structures to high-intensity dynamic loading. Int. J. Impact Eng. **35**(9), 1063–1074 (2008). https://doi.org/10.1016/j.ijimpeng.2007.06.008
31. K. Spranghers, I. Vasilakos, D. Lecompte, H. Sol, J. Vantomme, Numerical simulation and experimental validation of the dynamic response of aluminum plates under free air explosions. Int. J. Impact Eng. **54**, 83–95 (2013). https://doi.org/10.1016/j.ijimpeng.2012.10.014
32. S.M. Nelson, B.J. O'Toole, Computational analysis of blast loaded composite cylinders. Int. J. Impact Eng. **119**(April), 26–39 (2018). https://doi.org/10.1016/j.ijimpeng.2018.04.013
33. S.E. Rigby et al., Observations from preliminary experiments on spatial and temporal pressure measurements from near-field free air explosions. Int. J. Prot. Struct. **6**(2), 175–190 (2015). https://doi.org/10.1260/2041-4196.6.2.175
34. S.C.K. Yuen, A. Butler, H. Bornstein, A. Cholet, The influence of orientation of blast loading on quadrangular plates. Thin-Walled Struct. **131**(April), 827–837 (2018). https://doi.org/10.1016/j.tws.2018.08.004
35. N.S.A. Razak, A. Alias, N.M. Mohsan, S.A. Masjuki, The influence of Cowper–Symonds coefficients on the response of stiffened steel plates subjected to close-in blast loads. Key Eng. Mater. **912**, 171–184 (2022)
36. S. Jia, Q. Tan, J. Ye, Z. Zhu, Z. Jiang, Experiments on dynamic mechanical properties of austenitic stainless steel S30408 and S31608. J. Constr. Steel Res. **179**, 106556 (2021). https://doi.org/10.1016/j.jcsr.2021.106556
37. C. Zhang, P.J. Tan, Y. Yuan, Confined blast loading of steel plates with and without pre-formed holes. Int. J. Impact Eng. **163**(December 2021), 104183 (2022). https://doi.org/10.1016/j.ijimpeng.2022.104183
38. S.S. Hsu, N. Jones, Quasi-static and dynamic axial crushing of thin-walled circular stainless steel, mild steel and aluminium alloy tubes. Int. J. Crashworthiness. **9**(2), 195–217 (2004). https://doi.org/10.1533/ijcr.2004.0282
39. N. Jones, C. Jones, Inelastic failure of fully clamped beams and circular plates under impact loading. Proc. Inst. Mech. Eng. Part C J. Mech. Eng. Sci. **216**(2), 133–149 (2002). https://doi.org/10.1243/0954406021525070
40. J. Yu, N. Jones, Further experimental investigations on the failure of clamped beams under impact loads. Int. J. Solids Struct. **27**(9), 1113–1137 (1991). https://doi.org/10.1016/0020-7683(91)90114-U

41. F. Li, H. Yuan, H. Liu, Implementation of metal ductile damage criteria in Abaqus FEA. J. Phys. Conf. Ser. **1**, 2021 (1906). https://doi.org/10.1088/1742-6596/1906/1/012058
42. M. Li, Z. Zong, L. Liu, F. Lou, Experimental and numerical study on damage mechanism of CFDST bridge columns subjected to contact explosion. Eng. Struct. **159**(January), 265–276 (2018). https://doi.org/10.1016/j.engstruct.2018.01.006
43. Y. Bao, Dependence of ductile crack formation in tensile tests on stress triaxiality, stress and strain ratios. Eng. Fract. Mech. **72**(4), 505–522 (2005). https://doi.org/10.1016/j.engfracmech.2004.04.012
44. M.A. Iqbal, K. Senthil, P. Bhargava, N.K. Gupta, The characterization and ballistic evaluation of mild steel. Int. J. Impact Eng. **78**, 98–113 (2015). https://doi.org/10.1016/j.ijimpeng.2014.12.006
45. A. Das, T. Chowdhury, S. Tarafder, Ductile fracture micromechanisms of high strength low alloy steels. Mater. Des. **54**, 100–1009 (2014). https://doi.org/10.1016/j.matdes.2013.09.018
46. X. Liu, S. Yan, K.J.R. Rasmussen, G.G. Deierlein, Verification of void growth-based exponential damage function for ductile crack initiation over the full range of stress triaxialities. Eng. Fract. Mech. **269**(January), 108571 (2022). https://doi.org/10.1016/j.engfracmech.2022.108571
47. J. Trajkovski, R. Kunc, J. Perenda, I. Prebil, Minimum mesh design criteria for blast wave development and structural response: MMALE method. Lat. Am. J. Solids Struct. **11**(11), 1999–2017 (2014). https://doi.org/10.1590/S1679-78252014001100006
48. A.A. Nassr, A.G. Razaqpur, M.J. Tait, M. Campidelli, S. Foo, Experimental performance of steel beams under blast loading. J. Perform. Constr. Facil. **26**, 600–619 (2012)
49. W. Xiao, M. Andrae, N. Gebbeken, Air blast TNT equivalence concept for blast-resistant design. Int. J. Mech. Sci. (2020). https://doi.org/10.1016/j.ijmecsci.2020.105871
50. D. Bogosian, M. Yokota, S. Rigby, TNT equivalence of C-4 and PE4: a review of traditional sources and recent data, in *24th Int. Symp. Mil. Asp. Blast Shock (MABS 24)*, no. September, pp. 1–15 (2016)
51. A. Markose, C.L. Rao, Failure analysis of V-shaped plates under blast loading. Procedia Eng. **173**, 519–525 (2017). https://doi.org/10.1016/j.proeng.2016.12.080